Transport of Asian ozone pollution into surface air over the western United States in spring

Meiyun Lin[1, 2], Arlene M. Fiore[2,3], Larry W. Horowitz[2], Owen R. Cooper[4,5], Vaishali Naik[2,6], John Holloway[5], Bryan J. Johnson[5], Ann M. Middlebrook[5], Samuel J. Oltmans[4], Ilana B. Pollack[4,5], Tomas B. Ryerson[5], Juying X. Warner[7], Christine Wiedinmyer[8], John Wilson[2], Bruce Wyman[2]

[1]Atmospheric and Oceanic Sciences, Princeton University, 201 Forrestal Road, Princeton, NJ 08540, USA
[2]NOAA Geophysical Fluid Dynamics Laboratory, Princeton, NJ 08540, USA
[3]Now at Earth and Environmental Sciences, Columbia University and Lamont-Doherty Earth Observatory, Palisades, New York
[4]Cooperative Institute for Research in Environmental Sciences, University of Colorado, Boulder, Colorado
[5]NOAA Earth System Research Laboratory, Boulder, Colorado
[6]High Performance Technologies, Inc, NOAA Geophysical Fluid Dynamics Laboratory, Princeton, New Jersey
[7]Joint Center for Earth Systems Technology, University of Maryland Baltimore County, Maryland
[8]National Center for Atmospheric Research, Boulder, Colorado

Corresponding Author:

Meiyun Lin
meiyunl@princeton.edu
(609) 452-6551

Draft: 2011-09-30
Submitted to JGR-Atmosphere, CalNex Special Section

Abstract

Many prior studies clearly document episodic Asian pollution in the western U.S free troposphere. Here, we examine the mechanisms involved in the transport of Asian pollution plumes into western U.S. surface air through an integrated analysis of *in situ* and satellite measurements in May-June 2010 with a new global high-resolution (~50x50 km^2) chemistry-climate model (GFDL AM3). We find that AM3 with full stratosphere-troposphere chemistry nudged to reanalysis winds successfully reproduces sharp ozone gradients above California due to the interleaving and commingling of Asian pollution and stratospheric air associated with mid-latitude cyclone passages. Asian pollution descends isentropically behind cold fronts, with a maximum enhancement to ozone at ~800 hPa occurring over the southwestern U.S., including the densely populated Los Angeles Basin. During strong episodes, Asian emissions can contribute 8-15 ppbv on days when peak observed daily maximum 8-hour average ozone (MDA8 O_3) levels are above 60 ppbv. We find that in the absence of Asian anthropogenic emissions, 20% of MDA8 O_3 exceedances of 60 ppbv in the model would not have occurred in the southwestern USA. For a 70 ppbv threshold, that statistic is 49%. Our analysis highlights the potential for trans-Pacific transport to contribute to high surface ozone episodes over the western USA. We further demonstrate a proof-of-concept approach using near real-time space-based CO measurements to identify strong Asian pollution plumes off the U.S. west coast and to serve at least as a qualitative early-warning indicator (lead time of 1-2 days) for the Asian enhancements to western U.S. surface ozone.

1 Introduction

A synthesis of available observations indicates an increase of springtime ozone (O_3) mixing ratios in the free troposphere and at surface sites of the western United States since the 1980s [*Jaffe et al.,* 2003; *Oltmans et al.,* 2008*; Parrish et al.,* 2009; *Cooper et al.,* 2010], coincident with rising Asian anthropogenic emissions of O_3 precursors as inferred from satellite measurements of column NO_2 and bottom-up inventories [*e.g. Richter et al.,* 2005; *Ohara et al.,* 2007; *Q. Zhang L. et al.,* 2009]. Global model simulations further support the role of rising Asian emissions in contributing to the springtime O_3 trend in the western U.S. [*Jacob et al., 1999; Zhang et al., 2008*]. Many prior studies clearly document episodic Asian pollution in the free troposphere over this region [*e.g. Jaffe et al.,* 1999; *Yienger et al.,* 2000; *Heald et al.,* 2003*; Jaegle et al.,* 2003*; Cooper et al.,* 2004a*; Goldstein et al.,* 2004; *Hudman et al.,* 2004; *Zhang et al.,* 2008]. The extent to which this pollution is entrained into the boundary layer is unclear [*Brown-Steiner and Hess,* 2011] yet has implications for attainment of U.S. air quality standards. Here, we seek greater understanding of the mechanisms that transport Asian pollution into western U.S. surface air through an integrated analysis of *in situ* and satellite measurements with a new high-resolution (~50x50 km^2) global chemistry-climate model (GFDL AM3) [*Donner et al.,* 2011]. In particular, we quantify the contribution of Asian pollution to surface O_3 levels on highly polluted days in both densely populated regions such as the Los Angeles (LA) Basin and in rural areas such as national parks.

Baseline O_3, as defined by the Task Force on Hemispheric Transport of Air Pollution (TF HTAP), is the observed O_3 at a site when it is not influenced by recent, locally emitted or produced anthropogenic pollution [*TF HTAP*, 2010]. The

rising Asian component of U.S. baseline O_3 poses an additional challenge to meeting more stringent National Ambient Air Quality Standard (NAAQS) for O_3 [*Lefohn, et al.,* 1998; *Fiore et al.,* 2002; *Keating et al.*, 2004]. The U.S. primary NAAQS for O_3, based on the 4th highest daily maximum 8-hour average O_3 (MDA8 O_3) concentration in surface air averaged over three years, may decrease from a threshold of 75 ppbv to one in the range of 60-70 ppbv [*Federal Register, 2010*]. The U.S. EPA estimates a doubling of violating counties across the USA if a 60 ppbv threshold is adopted (based on the 2006-2008 monitoring data, http://www.epa.gov/air/ozonepollution/pdfs/20100104maps.pdf). Earlier work indicates that the contribution of Asian emissions to surface O_3 in the U.S. reflects mostly an enhancement in background levels [e.g. *Goldstein et al*., 2004; *Zhang et al.,* 2008], and generally decreases on highly polluted days in summer [*e.g. Fiore et al.,* 2002]. However, a few recent studies suggest a correlation between baseline O_3 entering the U.S. west coast and local pollution episodes in California [*e.g. Parrish et al.,* 2010; *Huang et al.,* 2010; *Pfister et al.,* 2011]. While these studies provide useful information on baseline O_3 impacting the western U.S. surface, quantitative estimates of baseline O_3 levels, including its temporal and spatial variability throughout the country, are needed to inform the NAAQS-setting process and the development of effective state implementation plans (SIPs; the process by which states demonstrate their path to achieving compliance with the NAAQS).

Pollution transported from Asia to North America originates in the boundary layer of East Asia, where primary air pollutants are directly emitted from combustion and industrial sources. The polluted air masses are exported from the Asian boundary layer to the free troposphere via large-scale lifting such as deep

convection or warm conveyor belts embedded in mid-latitude cyclones [*e.g. Carmichael et al.,* 2003; *Liu et al.,* 2003; *Cooper et al.,* 2004; *Lin et al.,* 2010] as well as via meso-scale processes such as orographic forcing and mountain-chimney effects [e.g. *Chen et al.,* 2009; *Ding et al.,* 2007]. The exported pollutants traverse the North Pacific Ocean in the mid- and upper troposphere, and eventually descend towards the surface [e.g. *TF HTAP* 2010; *Brown-Steiner and Hess*, 2011 and references therein]. Earlier work suggests that only a small portion (<10%) of the Asian pollutants reaching the North American free troposphere descends into surface air [*Yienger et al.,* 2000*; Cooper et al.,* 2004; *Zhang L. et al.,* 2009]. However, these prior estimates, based on global-scale chemical transport models (CTMs) or Lagrangian trajectory models, both driven with meteorological fields typically at 2°x2° horizontal resolution, may be conservative as new evidence suggests an important role for meso-scale processes (e.g. mountain-valley flows, land-sea interactions, and boundary layer turbulence) in the exchange of air masses between the boundary layer and the free troposphere [*e.g. Chen et al.,* 2009; *Parrish et al.,* 2010]. The dilution of intense plumes due to numerical diffusion in global-scale models further diminishes the impacts of vigorous episodic transport events [e.g. *Lin et al.,* 2010; *Rastigejev et al.,* 2010 *and references therein*].

An additional goal of this study is to extend earlier efforts that developed meteorological indices to characterize the daily to interannual strength of Asian pollution outflow and trans-Pacific transport [*Liu et al.,* 2005, *Liang et al.,* 2005]. We hypothesize that space-based instruments are useful for developing these indices given their vast spatial coverage at near-daily intervals and their ability to capture variability in chemical composition associated with synoptic-scale

weather patterns. Over the last decade, satellite remote sensing has been widely used to advance our understanding of large-scale outflow of carbon monoxide (CO) from major biomass-burning regions [e.g. *Edwards, et al,* 2003; *McMillan et al.,* 2005; *McMillan et al.,* 2008], pollution transport to the Arctic [e.g. *Stohl et al*., 2007], intercontinental transport of air pollution [e.g. *Heald et al.,* 2003; *Zhang et al.,* 2008; *Pfister et al.,* 2011], and natural dust [e.g. *Chin et al.,* 2007; *Uno et al.,* 2009; *Li et al.,* 2010]. Specifically, we explore the potential for near real-time space-based measurements of CO columns to help inform regional air quality management decisions regarding the potential for Asian pollution to enhance surface O_3 concentrations over the western USA.

Section 2 briefly describes the model simulations and observational data. We focus our analysis on May-June 2010, leveraging intensive *in situ* vertical profiling of O_3 and related species during the NOAA CalNex (Research at the Nexus of Air Quality and Climate Change) field campaign in California (*http://www.esrl.noaa.gov/csd/calnex*). Section 3 examines the transport pathways of Asian pollution over the western U.S., including the influence of mid-latitude cyclones, commingling of Asian polluted air masses with stratospheric air, and isentropic transport mechanisms. A summary of model evaluation is reported in Section 4. Section 5 presents the average impacts of Asian anthropogenic emissions on U.S. surface O_3 and its contribution to high-O_3 events during the CalNex period. Section 6 illustrates a proof-of-concept approach developing a space-based index to identify situations under which episodic Asian pollution plumes may affect surface O_3 air quality over the western USA.

2 Measurements and Model

2.1 Meteorological and chemical environment in May-June 2010

The Asian contribution to O_3 in the western U.S. is affected by the amount of O_3 produced in the Asian boundary layer, by the strength and position of the North Pacific storm track, and by additional O_3 produced during transport. May-June is the beginning of the O_3 pollution season at northern mid-latitudes, with the East Asian coast experiencing maximum O_3 concentrations prior to the onset of the East Asian summer monsoon [e.g.*Tanimoto et al.,* 2005; *Lin et al.,* 2009]. According to the NOAA Climate Prediction Center (http://www.cpc.ncep.noaa.gov), the 2009-2010 winter was influenced by strong El Niño conditions. Upper level frontal and associated folding events over the western U.S. are typically enhanced in the late spring following an El Niño winter. Indeed, the ridge-trough pattern over the eastern North Pacific and western U.S. was amplified during May-June 2010, resulting in stronger surface anticyclones and northwesterly surface winds relative to climatology [*Cooper et al.,* 2011]. Furthermore, *Koumoutsaris et al* [2008] show that springtime Asian pollution outflow was enhanced in 1998 due to changes in convective activity in East Asia as well as the strengthening and eastward extension of the North Pacific storm track following an El Niño. We therefore expect that meteorological conditions during spring 2010 led to a particularly active season for export of Asian pollution and its subsequent transport to North America. These conditions, in conjunction with vast observations collected during the CalNex campaign (Section 2.2), offer an invaluable opportunity to improve our mechanistic understanding of Asian pollution transport.

2.2 *In situ* measurements

During the CalNex campaign, near-daily ozonesondes were launched at six sites

in California (auxiliary Fig. S1) between May 10 and June 19, 2010, to measure baseline O_3 at the U.S. west coast [*Cooper et al.,* 2011]. For comparison with measurements, we sample AM3 at the location and times of sonde launches and interpolate them to sonde pressure and then group them into 0.5 km altitude bins. Three-hourly model fields are used, linearly interpolated to the sonde launch times (14:00-16:59 Pacific Daylight Time). We also use collocated measurements of O_3, NO_x, NO_y, CO, sulfate and organic aerosols aboard the NOAA WP-3D aircraft during CalNex to characterize Asian pollution layers above California (Section 3.3) and to evaluate the model (Section 4). Measurement techniques are described in prior publications [*Ryerson et al.*, 1998; *Holloway et al.,* 2000; *Drewnick et al.*, 2005; *Bahreini et al*., 2010]. For ground-level O_3, we compare daily maximum 8-hour average O_3 (hereafter MDA8 O_3) sampled at the model surface layer with observations from the U.S. EPA's Clean Air Status and Trends Network (CASTNet) and Air Quality System (AQS) database. For all model comparisons to *in situ* measurements, we apply bilinear horizontal interpolation (using the nearest four model grid cells) when sampling model fields.

2.3 Satellite data

We use observations of CO and O_3 total column amounts from the Atmospheric Infrared Sounder (AIRS) onboard the NASA Aqua satellite to identify trans-Pacific Asian pollution events and stratospheric O_3 intrusions, respectively. The AIRS cross-track scanning grating spectrometer coupled with the Aqua cross-track scanning Advanced Microwave Sounding Unit (AMSU) provides vertical profiles of the atmosphere with a nadir 45 km field of regard (FOR) across a 1650 km swath [*Aumann et al*., 2003]. The broad swath, infrared spectral coverage, and reconstructed cloudy pixels [*Susskind et al*., 2003] of AIRS enable retrievals over

nearly 70% of the planet every day with substantial portions of the globe observed twice daily (ascending and descending orbits), thus providing a unique opportunity for process studies of synoptic-scale chemical transport in the global atmosphere [*McMillan et al., 2005; McMillan et al., 2008*]. In this study we use version 5.2 Level 3 daily 1°x1° gridded standard products (AIRX3STD) of AIRS CO [*McMillan et al., 2011*] and O_3 total column retrievals [*Susskind et al*., 2003], downloaded from the NASA Goddard Earth Sciences Data and Information Services Center (*http://disc.sci.gsfc.nasa.gov/*). The ascending and descending retrievals are combined to provide better spatial coverage.

The main sensitivity of AIRS to tropospheric CO occurs between approximately 300-600 hPa, and both V4 and V5 CO retrievals at 500 hPa are accurate within10% in the Northern Hemisphere [*McMillan et al.,* 2005; *Warner et al.,* 2007; *McMillan et al.,* 2008]. A number of validation exercises reveal that AIRS O_3 profile retrievals capture the large-scale dynamic variability and gradients of O_3 in the extratropical UT/LS region [*Monahan et al*., 2007; *Pan et al.*, 2007; *Pittman et al.*, 2009; *Wei et al*., 2010].

2.4 GFDL AM3 model simulations

AM3 is the atmospheric component of the GFDL global coupled atmosphere-oceans-land-sea ice model (CM3) [*Donner et al*., 2011; *Griffies et al.,* 2011]. The AM3 cubed-sphere grid greatly improves polar representation and computational efficiency [*Putman and Lin,* 2007]; the model's horizontal resolution is denoted as Cn, where n is an integer number indicating total number of cells (finite volumes) along each edge of the cube. We apply C180 (where the size of the grid cell varies from 43 km at the 6 corners of the cubed sphere to 62 km near the center

of each face) and C48 (163 - 231 km) horizontal resolution. Model simulations at the C48 resolution starting in January 2009 were used to initialize the C180 simulations spanning January - June 2010. Both coarse- and high-resolution simulations employ the same physical parameterizations and include 48 vertical levels, ranging in thickness from 70 m near the Earth's surface to 1-1.5 km near the tropopause and 2-3 km in much of the stratosphere.

AM3 includes a fully coupled stratosphere-troposphere-aerosol chemistry within a general circulation model. The chemistry models of *Horowitz* et al. [2003] for the troposphere and *Austin and Wilson* [2006] for the stratosphere are merged. We implement a stratospheric O_3 tracer by defining O_3 above the WMO thermal tropopause each model time step as "stratospheric" (O_3-strat), with its transport into the troposphere driven by dynamic processes (such as tropopause folds and cut-off lows). Once mixed into tropospheric air, O_3-strat is subject to transport and loss (chemical and depositional) in the same manner as O_3 of tropospheric origin. This technique likely overestimates the stratospheric contribution since any O_3 above the tropopause instantly gets labeled as "stratospheric" regardless of its actual origin.

AM3 is typically run in the climate mode, forced with prescribed sea surface temperatures (SSTs) and sea ice [e.g. *Austin and Wilson* 2010; *Golaz et al.,* 2011*; Fang et al.,* 2011; *Rasmussen et al.,* 2011] or as a component in the GFDL coupled model CM3 [*Griffies et al.,* 2011]. To enable direct comparisons with CalNex observations, AM3 simulations at both C48 and C180 horizontal resolution in this study are forced with observed SSTs as in the standard climate simulations, but horizontal winds are nudged to those from the NCEP Global

Forecasting System (GFS) at T85 horizontal resolution (approximately 1.4°x1.4°, archived 3 hourly) [*Kanamitsu et al.,* 1991]. Our goal is to preserve the large-scale features of the observed airflow while allowing AM3 to simulate meso-scale patterns, similar to the approach taken for high-resolution regional weather forecasting [*e.g. Skamarock et al.,* 2008; *Lin et al.,* 2009; *Lin et al.,* 2010] and hurricane modeling [*Knutson et al., 2008*]. The GFS model has 64 sigma levels with a model top at ~0.32 hPa, while the vertical coordinates of AM3 extend further into the mesosphere (~0.01 hPa). Further, to minimize the impacts of noise introduced via nudging, which has been shown to lead to excessive stratosphere-to-troposphere O_3 transport [*van Noije et al*., 2004 and references therein], we implemented a pressure-dependent nudging technique, relaxing the model to GFS U and V with a time scale of 6 hours in the surface level, but weakening the nudging strength with decreasing pressure (e.g., relaxing with a time scale of ~60 hours by 100 hPa and ~600 hours by 10 hPa). No nudging is implemented above ~10 hPa.

The impact of Asian emissions is determined as the difference between a base simulation with all emissions included, and a sensitivity simulation with the East Asian (15°-50°N, 95°-160°E) anthropogenic emissions (including aerosol) shut off in the model. Methane is set to observed values as a lower boundary condition in both simulations. The sensitivity simulation begins in January 2009 with the C48 horizontal resolution, allowing for a one-year spin-up period sufficient to capture changes in the background atmospheric composition due to Asian emissions. Horizontal winds in the sensitivity simulation are also nudged to the GFS winds, thus we expect that the large-scale transport should be similar between the two simulations although completely removing Asian emissions may induce some

feedbacks on hydrological processes (particularly through aerosol-cloud interactions which are included in AM3). Further, the O_3 response to emission perturbations is non-linear due to chemistry as discussed in *Wu et al*. [2009], who found that the perturbation from a 100% NO_x emission reduction yields O_3 responses greater than 5 times the 20% NO_x emission reductions. Differencing O_3 mixing ratios with sharp gradients in the vicinity of tropopause folds may also introduce noise. Therefore, for each event discussed, we carefully checked for consistent patterns in Asian enhancements to O_3, CO, and NO_y in the model, constrained wherever possible by independent observations (e.g. satellite images and ozonesondes).

2.5 Emissions

We implement emission inventories to reflect 2010 conditions. All emission inventories described here are regridded to 1°x1° for C48 and 0.5°x0.5° for C180. The global emissions from anthropogenic sources and international shipping for the year 2000 (0.5°x0.5°) were taken from *Lamarque et al* [2010] as a base inventory. We then replaced anthropogenic emissions in the East Asian domain (13°S-53°N, 70°-150°E) with the 2006 Asian emission inventory (0.5°x0.5°) from Q. *Zhang et al*. [2009], scaled to 2010 as described below, and the North American (24°-60°N, 135°-40°W) emissions with the U.S. National Emission Inventory (NEI) for 2005 (4 x 4 km^2) (ftp://aftp.fsl.noaa.gov/divisions/taq/emissions_data_2005).

We increase the Chinese NO_x emissions in *Q. Zhang et al.* [2009] by 32.6% for 2010 and 27.9% for 2009, based on changes in the 2006-2010 satellite measurements of NO_2 columns over central eastern China (30°-40°N, 110°-

123°E) from the SCIAMACHY sensor (available on www.tenis.nl, with retrieval technique previously described by *Boersma et al* [2004]). Our estimate reflects the relatively lower rate of increase of Chinese NO_x emissions during the economic downturn of 2009-2010 [J.-T. *Lin et al*., 2011] as compared to earlier years [Q. *Zhang et al.*, 2009]. Using NO_2 columns directly will tend to overestimate changes in emissions over polluted regions since an increase in NO_x emissions consumes OH and increases the NO_x lifetime, but underestimate changes in emissions over remote regions where an increase in NO_x emissions decreases the NO_x lifetime through feedbacks on O_3 and OH [*Lamsal et al.*, 2011]. Indeed, our estimate for the 2006-2009 emission trend (+27.9%) based on NO_2 columns over polluted central eastern China is ~9% higher than that reported in *Lamsal et al*. [2011] who considered the influence of NO_x lifetime when deriving emission changes from SCIAMACHY measurements of NO_2 columns.

We also increase NMVOC emissions in China by 23.2% for 2010 and 17.4% for 2009, relative to 2006, assuming the same annual growth rate as 2001-2006 previously reported by Q. *Zhang et al.* [2009], due to lack of better information. Emissions of SO_2, CO, black carbon and organic carbon remain at the 2006 level, based on recent evidence from satellites [*Lu et al.,* 2010; *Lei et al.,* 2010; personal communication with *D. G. Streets,* 2010].

Daily biomass burning emissions for 2009-2010 are adopted from *Wiedinmyer et al.* [2011] (FINN v1, 1 x 1 km^2) and distributed over six ecosystem-dependent altitude regimes between the surface and 6 km, following the recommendations of *Dentener et al.* [2006]. Isoprene emissions from vegetation are calculated

online based on the Model of Emissions of Gases and Aerosols in Nature (MEGAN) [*Guenther et al.,* 2006], as implemented in *Emmons et al.* [2010] with modifications described by *Rasmussen et al*. [2011]. Other natural emissions -- including acetone, ethane, propane, ethylene, propene, methanol, ethanol and monoterpenes from vegetation, CO from vegetation and ocean, volcanic SO_2, soil and lightning NO_x, dimethyl sulfide (DMS), sea salt and dust -- are included as in the standard AM3 simulation [*Donner et al.,* 2011].

3 Transport pathways of Asian pollution

We identify three major trans-Pacific Asian pollution events from AIRS measurements of daily CO columns for May-June 2010. Figure 1 illustrates the daily progression of these large-scale CO plumes from the East Asian coast to the North American west coast during May 4-8, May 16-20, and June 15-19. The June plume (Fig.1c) took a more northerly route to the Gulf of Alaska followed by southeastward advection towards southern California, spending ~1 day longer over the North Pacific Ocean than the two plumes in May. Model CO columns exhibit a similar large-scale structure as the AIRS data, and reveal that these CO plumes are dominated by Asian pollution which was lofted from the continental boundary layer of eastern China approximately 1 week prior to their arrival to the U.S. west coast (figure not shown). Our analysis described below mainly revolves around the three Asian pollution events displayed in Fig. 1, the mechanisms governing their transport into western U.S. surface air, and the ability of AM3 to capture these processes.

3.1 Cyclone passages and merging air streams

Prior work has shown that Asian pollution is often intermingled with stratospheric

O_3 intrusions above the North American west coast [e.g. *Jaegle et al.,* 2003; *Cooper et al.*, 2004b]. Indeed, we find that deep tropopause folds occurred one day prior to the arrival of Asian pollution above the California coast on May 18 and June 17, while the May 4-8 pollution event was followed by two consecutive stratospheric intrusions on May 9-11. Taking the May 16-20 event as an example, we examine here the dynamic processes leading to the interleaving and commingling of Asian and stratospheric originating air masses associated with mid-latitude cyclones over the eastern North Pacific. A combination of satellite images, ozonesondes, and three-dimensional model simulations is used to illustrate these processes.

Figure 2 depicts the evolution of two consecutive mid-latitude cyclones sweeping over the Gulf of Alaska and the associated upper level structure during May 17-19. On May 17, AIRS-retrieved total O_3 shows a sharp spatial gradient, with a narrow band of elevated O_3 columns in excess of 450 DU (Fig.2d) coinciding with an elongated dry air stream in the GFDL AM3 model (Fig.2a), both extending to the California coast. This typical feature of a stratospheric intrusion [*Wimmers et al.*, 2003; *Felker et al*., 2011] is also represented in the GFS Final (FNL) analysis by the potential vorticity (PV) contours on the 300 hPa surface. The ozonesonde launched at Point Reyes, located immediately to the right of the tropopause fold off the California coast, recorded high O_3 mixing ratios in excess of 100 ppbv penetrating down as low as 6 km a.s.l. (Fig. 3a), coincident with low humidity, a marker for air of stratospheric origin.

Between May 17-18, this dry air stream of stratospheric origin sheared into three components in a similar manner previously described by *Cooper et al*. [2004b].

Depicted in the AIRS retrievals of total column O_3 and model upper level humidity on May 18 (Fig. 2, middle panels), the first component travels across the western U.S. with the upper level flow, while the second component representing the bulk of the dry air stream moves northward. A three dimensional view of AM3 stratospheric O_3 tracer reveals that the third component descends isentropically into the lower troposphere, leading to the formation of a distinct O_3 layer just 2 km above the California coast by 21:00 UTC, May 18 (Fig. 4a and Fig. S2). Transported stratospheric remnants contribute 40-80 ppbv to the simulated 60-100 ppbv range of total O_3 mixing ratios in this approximately 2 km thick layer of enhanced O_3, with minimal influence (<10 ppbv) from Asian emissions. AIRS observations of CO columns indicate transport of an Asian pollution plume into the eastern North Pacific on May 18 by the warm conveyor belt (WCB) of the next mid-latitude cyclone entering this region (Fig. 1a). We find in the model that the bulk of Asian polluted air masses were located in the upper troposphere (6-10 km) (Fig. 4d), immediately adjacent to stratospheric air on the left (Fig. 4a). Asian anthropogenic emissions contribute 20-30% of total O_3 mixing ratios in the upper troposphere when the air was sampled by the Point Reyes ozonesonde on May 18 (Fig.3b). Similar to the findings of *Stohl and Trickl* [1999], these processes reveal two interleaving O_3 layers with dominating stratospheric and Asian influence in the lower and upper troposphere, respectively, as observed by the ozonesondes launched along the California coast on May 18 (auxiliary Fig. S2).

By 21:00 UTC, May 19, the first cyclone decayed and a newly formed cyclone was located off the coast of Washington (Fig. 2c). A portion of stratospheric air that had rolled back from the deep intrusion on May 17 was now entrained into the newly formed tropopause fold of the second cyclone. AIRS shows dispersed

CO enhancements in the vicinity of the spiraling WCB above the Washington coast on May 19 (Fig. 1b) along with elevated total O_3 columns (Fig. 2f), suggesting the intermingling of polluted and stratospheric air. Consistent with these features observed from space, AM3 model simulations show collocated high mixing ratios of stratospheric O_3 tracer and Asian CO in the mid- and upper troposphere above the U.S. west coast (Fig. 4, middle panels). A distinct high-O_3 layer with lower humidity between 4-8 km a.s.l. was observed by the Point Reyes and Point Sur ozonesondes and successfully captured by the model (Fig. 3c and d). In the ~60-95 ppbv of simulated total O_3 in this layer, remnants of stratospheric intrusions and Asian anthropogenic emissions contribute ~40-55 ppbv and 10-25 ppbv, respectively.

By 21:00 UTC, May 20, stratospheric and Asian polluted air masses became further intermingled and descended into the mid- and lower troposphere above southern California (Fig. 4, right panels). These air masses reached the western U.S. surface on May 20-21 under the influence of a surface anticyclone, contributing to elevated surface O_3 episodes in the national parks (Section 5.2).

Other stratospheric intrusions identified during the CalNex campaign were also mixed, to varying degrees, with Asian pollution, suggesting that the dispersion of O_3-rich stratospheric air into polluted air masses is a common feature in the vicinity of active storm tracks in the North Pacific as well as in the Atlantic [e.g., *Stohl and Trickl*, 1999; *Parrish et al., 2000*; *Esler et al*., 2003]. Our analysis further supports prior publications suggesting that a positive O_3-CO correlation does not necessarily indicate anthropogenic influence on O_3 enhancements in the continental outflow (such as Asian Pacific Rim) or inflow regions (such as

North American west coast) [*Cooper et al*., 2004b; *Voulgarakis et al.,* 2011]. Thus the O_3-CO correlations derived from collocated *in situ* or satellite measurements (such as TES) reported in earlier studies [e.g., *Zhang et al.,* 2006*; Zhang et al.,* 2008*; Voulgarakis et al.,* 2011*; Pfister et al.,* 2011] should be interpreted with caution.

3.2 Isentropic transport mechanisms

We explore here the role of synoptic vs. meso-scale processes in controlling the transport of Asian pollution into western U.S. surface air and its impacts on the regional variability in surface O_3, focusing on the Asian pollution event in June (Fig. 1c). Figure 5 shows observed and simulated O_3 profiles at Trinidad Head and Point Reyes on June 17-19, illustrating a layered structure of O_3 with stratospheric and Asian origin, similar to those discussed in Section 3.1. Less entrainment of stratospheric air into the polluted WCB occurs during this event (Fig.S3) than during May 19-20. During June 17-19, the large Asian influence on O_3 mixing ratios (up to 30 ppbv) mainly occurred between ~3-9 km above the California coast, coinciding with the observed layer of enhanced relative humidity.

AM3 suggests that this Asian pollution plume with enhanced tropospheric column O_3 entered the California coast on June 20 (Fig. 6), following transport across the North Pacific Ocean as seen from AIRS CO (Fig. 1c). The Asian enhancement to tropospheric column O_3 is calculated using the 150 ppbv O_3 "chemical tropopause" from daily mean data in the base simulation. Between June 19-20, a mid-latitude cyclone (centered along 45°-50°N) intensified and moved into the Gulf of Alaska, the eastern Pacific anticyclone shifted southeastward with its edge lying off the coast of California, and a weak surface

low extended northward from Mexico. This pressure gradient produced onshore flow, containing Asian pollution, across central and southern California. The lower panels of Fig. 6 depict two curtain plots transecting from north to south across the plume, revealing a strong latitudinal variation of Asian O_3 along isentropic surfaces. By 21:00 UTC, June 20, the plume has progressed to southern California, with the vertical distribution of Asian O_3 up to 10-30 ppbv exhibiting a continuous band sloping from 5-8 km a.s.l. all the way to the surface of the Sierra Nevada and southern California (Fig. 6, left panels). This isentropic descent is a typical feature of Asian plumes entering the western U.S. [*Brown-Steiner and Hess,* 2011]. A layer of elevated Asian O_3 was located immediately above a well-mixed boundary layer at 21:00 UTC, June 21 (Fig. 6, right panels). It is possible that the Asian O_3 in the lower free troposphere was entrained into surface air during the growth of the afternoon boundary layer.

Next, we calculate the Asian enhancements to MDA8 O_3 in surface air using the same 8-hour interval identified for the MDA8 in the base simulation (Fig. 7). Consistent with the strong descending motion of Asian polluted air masses depicted in Fig. 6, Asian anthropogenic emissions enhance MDA8 O_3 in surface air by up to 10-15 ppbv, primarily in the high-elevation regions downwind of subsiding plumes. We find that Asian anthropogenic emissions can contribute up to 15-20% of total O_3 in the model surface level over parts of the intermountain regions. The regions experiencing high Asian influence in excess of 10-15 ppbv extend across much of Colorado and New Mexico by June 22, consistent with the observed and simulated total O_3 pattern, suggesting an important role for Asian anthropogenic emissions in episodically enhancing surface O_3 levels above the surrounding “background”. The enhancement due to Asian emissions contributes

5-8 ppbv to MDA8 exceedances of the current 75 ppbv NAAQS in parts of southern California on June 22 and 8-15 ppbv to exceedances of a 60 ppbv threshold -- the lowest value proposed for an O_3 NAAQS reconsideration -- in the intermountain regions. While this estimate is likely an upper limit for current conditions (see discussion of non-linearities in O_3 chemistry and scaling of Chinese NO_x emissions in Section 2.4), it nevertheless indicates the potential for Asian emission to contribute to high-O_3 episodes over the high-altitude western United States, with implications for attaining more stringent NAAQS for O_3 in this region.

Asian influence appears to be minimal in the pronounced O_3 pollution exceeding 75 ppbv in the Central Valley of California on June 21-22. The O_3 pollution in the Central Valley mostly reflects photochemical production from local emissions and suppressed ventilation under the influence of a surface anticyclone. *Langford et al.* [2010] suggested that O_3 produced in the LA Basin can be transported to eastern Utah and western Colorado by topographic venting and westerly flow under a surface meteorological pattern similar to that depicted in Fig. 6. AM3, however, indicates that the southeastward shift in the locations experiencing peak surface O_3 values from June 20 to June 22 (Fig. 7) is instead caused by subsiding Asian pollution intersecting the elevated terrain of the western USA. To further explore this question, we conduct a sensitivity simulation with North American anthropogenic emissions switched off in the model. The results suggest that North American contributions mainly occurred in the Central Valley and no more than a 150 km radius around each city (e.g. Phoenix and Salt Lake City) during June 20-22 in our model (auxiliary Fig. S4). However, the ~50x50 km^2 horizontal resolution of AM3 may be insufficient to capture the meso-scale

mountain-valley flows described by *Langford* et al [2010]. Future work should employ models at even higher resolution to identify any role of topographical venting of pollution.

Another notable feature in Fig. 7 is the modeled O_3 minimum above the ocean that parallels the coast and varies strongly with distance from shore. This O_3 minimum largely reflects the influence of the low-level jet along the California coast which is typically at a maximum in summer [*Burk and Thompson*, 1996; *Parish*, 2000]. The lower observed O_3 at the AQS sites near the coast supports the existence of this transport pattern. Asian enhancements to O_3 in the coastal marine boundary layer do not exhibit strong episodic variations, consistent with prior publications regarding background influence at the Trinidad Head surface site [*Goldstein et al*., 2004; *Zhang L. et al.*, 2009; *Parrish et al.*, 2010; *Cooper et al.*, 2011]. Our results further reveal that the majority of the Asian pollution plumes arriving to the U.S. west coast are located in the free troposphere where a portion of the pollution descends isentropically behind cold fronts and eventually becomes entrained into the daytime boundary layer over land. This transport mechanism is the key driver for the stronger signal of episodic Asian pollution in surface air over the U.S. intermountain regions than the North Pacific Ocean.

3.3 Dispersion of Asian pollutants into southwestern U.S. surface air

We discuss in this section the potential impacts of Asian pollution in a densely populated region like the LA Basin, where Asian pollution can mix with high levels of locally produced O_3 pollution. The NOAA WP-3D intercepted a pollution layer approximately 2 km above the LA Basin on May 8, with 3-8 $\mu g/m^3$ sulfate aerosol,

555 <1 μg/m^3 organic mass, 150-175 ppbv CO, and 80-90 ppbv O_3 (Fig. 8). This
556 pollution layer was encountered three times (denoted as red arrows in Fig. 8c) by
557 the aircraft, and shows distinct sulfate enhancements, in contrast to the boundary
558 layer pollution with dominant signatures of primary emissions (such as organic
559 matter and CO). The observed high concentration of sulfate is unlikely from
560 oxidation of SO_2 emissions from diesel ships off California's coast since no
561 collocated strong enhancements in CO and other primary emissions are found in
562 these sulfate-dominated pollution layers. The presence of an aerosol layer
563 dominated by sulfate is a distinguishing feature of Asian pollution layers that have
564 been transported to the eastern North Pacific [*Brock et al., 2004; Peltier et al.,*
565 *2008; Dunlea et al., 2009*]. When a polluted air mass rises out of the Asian
566 boundary layer, the existing aerosol is washed out if precipitation occurs during
567 lifting, while the less-soluble gas phase compounds such as SO_2 are not entirely
568 removed. SO_2 that "escaped" wet removal during lifting is converted into sulfate
569 during subsequent trans-Pacific transport in the free troposphere. The result is an
570 enhanced sulfate-to-organic aerosol ratio in the eastern North Pacific air masses
571 influenced by Asian pollution. Indeed, AIRS CO retrievals confirm the occurrence
572 of large-scale trans-Pacific transport of Asian pollution during May 2-8 (Fig. 1a).
573 The plume arrived at the coast of California on May 8, evident both in AIRS CO
574 and in the AM3 model Asian enhancements to tropospheric column O_3 (Fig. 8a).
575 A vertical cross-section of model Asian O_3 in Fig.8b depicts a plume-like feature
576 of Asian O_3 enhancements in excess of 10-25 ppbv sloping from 3-6 km above
577 northern California to 2-3 km above the LA Basin where the air masses were
578 sampled by the WP-3D. Other WP-3D flights during CalNex also intercepted
579 sulfate-dominated aerosol layers above California, to varying degrees, on May 7,
580 May 24, and June 20. The model indicates Asian enhancements to O_3 mixing

ratios but fails to reproduce the magnitude of sulfate concentrations, likely due to excessive wash out during trans-Pacific transport consistent with an overestimate in precipitation [*Donner et al.,* 2011].

Our analysis suggests that the signature of Asian pollution enhancements in the lower troposphere of the densely populated LA Basin is sufficiently strong to be observed, such as through analysis of chemical composition demonstrated here. Daytime mixed layers in this region range from 1-4 km a.s.l. [*Langford et al*., 2010; *Cooper et al.*, 2011 and references therein]. Asian pollution ~2 km aloft is thus available to be entrained into the boundary layer and contributes to the local pollution burden. It should be noted that strong dilution may occur when Asian polluted air masses are dispersed into the boundary layer. For example, Figure 9 shows that much of Nevada experiences a pronounced maximum of Asian enhancements (10-15 ppbv) to surface O_3 on May 8, primarily reflecting the free tropospheric signal intersected by the elevated terrain. By May 9, Asian influence covers a larger spatial extent (including southern California), but the magnitude is weakened by a factor of two. Observed O_3 at the CASTNet and AQS ground stations exhibits a similar day-to-day variability in the spatial pattern as model surface O_3. Despite dilution, Asian emissions contribute at least 50% of the surface O_3 increases from May 8 to May 9 over Arizona and western Colorado.

4 Model evaluation

Generalizing from the process-oriented analysis in Sections 3.1-3.3, we find that the high-resolution GFDL AM3 model with fully coupled stratosphere-to-troposphere chemistry nudged to reanalysis winds successfully reproduces the observed day-to-day variability in the vertical gradient of baseline O_3 entering the

California coast (Figs. 3 and 5; S2 and S3) as well as the development of high-O_3 days in surface air and its regional variability over the western U.S. (Figs. 7 and 9). We conclude that the model captures the sources, chemistry and transport controlling the O_3 variability over this region. For most cases, AM3 at C48 horizontal resolution (~163-231 km) also captures the shape of O_3 profiles reflecting mainly a combined influence from stratospheric intrusions and Asian pollution (auxiliary Figs. S2-S3). The model bias in the upper troposphere above most sites increases when the ozonesondes are primarily influenced by stratospheric air. Part of this upper tropospheric O_3 bias is likely due to the limitation in the current model resolution (both C48 and C180) to adequately resolve the filamentary structure of tropopause folds, which results in sharp vertical and horizontal gradients in O_3 mixing ratios. A systematic evaluation of model O_3 profiles at seven ozonesonde sites during CalNex, including day-to-day variability and mean biases at different altitude ranges, will be presented in a follow-up paper [Lin, M., et al (2011), Springtime high surface ozone events over the western United States: Quantifying the role of stratospheric intrusions, manuscript in preparation; hereafter *Lin M.*, et al., 2011, in prep].

Figure 10 compares May-June 2010 mean MDA8 O_3 in surface air between AQS observations and model results. The model captures the regional variability of mean observed surface O_3 over the western U.S., including a minimum in the coastal areas and a maximum in the southern California and intermountain regions. Systematic positive biases of up to 10-25 ppbv occur at the coastal sites and in northern California. Model biases at CASTNet sites (Table 1) show a spatial pattern similar to those at AQS sites, with a relatively larger bias occurring at Mount Rainier National Park in Washington, Lassen Volcanic National Park

633 and Pinnacles in northern California. Despite the large bias, the model
634 reproduces much of the day-to-day variability in surface O_3 with correlation
635 coefficients ranging from 0.4-0.8 and standard deviations within 15% of those
636 observed for most CASTNet sites. The surface ozone bias (2-10 ppbv) is typically
637 smaller at the high-elevation sites over the intermountain regions, suggesting that
638 downward transport from the free troposphere is not likely to be the primary
639 cause of the surface O_3 bias. Supporting this conclusion, we find that the model
640 bias in surface O_3 at the high-elevation sites (>1.5 km) does not have a direct
641 relationship with the Asian enhancements (auxiliary Fig. S5b).
642
643 Next we evaluate the O_3 production efficiency (OPE), O_x vs. NO_z derived from
644 collocated measurements of O_3, NO_x, and NO_y aboard the WP-3D aircraft during
645 CalNex, over the LA Basin and the Central Valley, respectively (Fig. 11). Only
646 flight legs below 1.5 km (auxiliary Fig. S1) and points where NO_y is between 2
647 and 10 ppbv are included, so as to filter out fresh plumes and very aged air,
648 retaining only moderately polluted air masses. The observations suggest a
649 slightly smaller OPE in the LA Basin than Central Valley. The model captures this
650 urban vs. rural difference in OPE [*Trainer et al*., 1993; *Kleinman et al.*, 1994], with
651 the slope of O_x vs. NO_z linear least-squares correlation within ~10% of those
652 observed for both regions. The intercept of the correlation can be interpreted as a
653 background O_3 level [*Kleinman et al*., 1994]. We find that the intercept of O_x vs.
654 NO_z over the LA Basin in the model is close to that in the observations (Fig. 11a).
655 For the Central Valley (Fig. 11b), however, the intercept is ~10 ppbv higher in the
656 model, suggesting a possible problem in the boundary layer “background” O_3
657 level over this region. Auxiliary Figure S6 confirms that the bias gets worse in the
658 low tail of the cumulative probability distribution of O_3 in the Central Valley.

We conclude that the model has systematic positive biases in the northern California and coastal regions. While the source of this problem is yet unclear, it may reflect some combined influence from model limitation in resolving coastal gradients and sharp topography, an overestimate in the boundary layer "background" in these regions, oxidant production and loss (chemical and depositional), and NO_x emissions or lifetime.

5 Impacts of Asian pollution on U.S. surface ozone air quality

5.1 Mean distributions

Figure 12a shows the mean Asian anthropogenic enhancement to U.S. O_3 mixing ratios at ~800 hPa averaged over May-June 2010. A pronounced maximum of Asian enhancements to near-surface O_3 occurred over the southwestern U.S. in spring 2010. Increasing Asian influences in the lower troposphere towards the south mainly reflect a combined influence from isentropic subsidence (Section 3) and additional production of O_3 from NO_x released from the thermal decomposition of Asian PAN when the air warms as it descends (auxiliary Fig.S7). Earlier studies suggest that Asian pollution reaching the eastern North Pacific Ocean typically splits into northern and southern branches with the resumption of O_3 production due to PAN decomposition occurring in the southern branch [e.g. *Moxim et al*., 1996; *Heald et al*., 2003; *Hudman et al., 2004; Zhang et al., 2008*]. We find that this mechanism extends into the western U.S. during spring 2010 and contributes to the total Asian enhancement to surface O_3.

The spatial pattern of Asian enhancements at ~800 hPa is in general agreement with forward trajectory analysis of surface destinations of baseline air masses in

685 *Cooper et al.* [2011] for the same study period. Our results suggest that Asian
686 enhancements, along with stratospheric contributions [*Lin et al.,* 2011, in prep],
687 explain the latitudinal variation of O_3 vertical gradients observed in ozonesondes
688 along the California coast during CalNex [*Cooper et al.,* 2011]. Compared with
689 the springtime climatological pattern of Asian O_3 tracer results by *Brown-Steiner*
690 *and Hess* [2011], our results for May-June 2010 indicate a relatively larger Asian
691 influence in southwestern U.S. surface air, likely reflecting the influence of the
692 southeastward extension of the Pacific storm tracks following an El Niño (Section
693 2.1).
694
695 Figure 12b shows the mean Asian influence on MDA8 O_3 in the model surface
696 layer for May-June 2010. Trans-Pacific transport of Asian pollution has the
697 greatest impacts on surface O_3 in the high-elevation regions over the western
698 U.S., consistent with prior studies [e.g. *TF HTAP* 2011; *Brown-Steiner and Hess*,
699 2011; *Zhang et al.*, 2011], where the elevated terrain has a higher probability of
700 intersecting subsiding air masses behind cold fronts than lower elevation regions
701 such as the Central Valley of California and the eastern U.S. (Section 3). The
702 minimum Asian O_3 enhancement in surface air occurs in the Southeast U.S.
703 where the average transport in the lower troposphere advects air masses from
704 the Gulf of Mexico, limiting the influence of westerly transport, similar to
705 summertime transport conditions discussed in *Fiore et al.* [2002]. Results from
706 AM3 simulations at C48 horizontal resolution show a similar spatial pattern of
707 Asian influence both in the lower troposphere and in surface air over U.S.
708 (auxiliary Fig. S8), but produce a 1-2 ppbv smaller impact at the surface in Utah,
709 Arizona and western Colorado than the C180 high-resolution simulations.
710

5.2 Contribution to air quality exceedances

We next examine the O_3 enhancement from Asian anthropogenic emissions for the entire distribution of springtime MDA8 O_3 concentrations in the model surface layer over the southwestern U.S. box in Fig. 12a. Figure 13 shows the Asian enhancements of up to 10-15 ppbv when springtime total O_3 concentrations exceed 70 ppbv over the polluted southern California and Arizona, consistent with case study results in Section 3 (gray points in Fig. 13). This finding is in contrast to an earlier study indicating that foreign influence typically declines below 8 ppbv in the 70-90 ppbv range of U.S. summertime total O_3 concentrations in surface air [*Fiore et al.*, 2002]. While local emissions likely play a dominant role in producing the high-O_3 events in surface air over this region, here we calculate the number of O_3 events in excess of 60 and 70 ppbv thresholds that would not have occurred in the model in the absence of Asian pollution enhancements. These points are denoted by the green and red trapezoids in Fig. 13 for 60 and 70 ppbv thresholds, respectively. We include only points where the Asian enhancement is above the 25th percentile to filter out model noise. Dividing the number of points falling within these trapezoids by the total number of points exceeding the threshold value, we estimate that 20% of MDA8 O_3 exceedances of 60 ppbv in the model would not have occurred over southern California and Arizona in the absence of Asian anthropogenic emissions. For a 70 ppbv threshold, this statistic increases to 49% since both the mean and extreme events of Asian enhancements increase in the 70-80 ppbv range of total O_3 and the number of exceedances for the 70 ppbv threshold decreases as compared with the 60 ppbv threshold.

We further examine any influence of model biases on the relationship between

Asian enhancements and total O_3 abundances, and thereby our estimate of the relative contribution to high-O_3 events. The results are reported in auxiliary Figure S5a for all AQS sites within the same region used in Fig. 13, suggesting no direct relationship (r^2=0.02) between Asian enhancements and model bias in surface O_3. *Reidmiller et al.* [2009] found an anti-correlation between foreign influence and model biases for a 15-model average (year 2001), and thus suggested that global models may underestimate foreign contribution. We do not find any evidence for this relationship in our model.

Next we explore the influence of Asian emissions on high-O_3 episodes at three representative CASTNet sites (Fig. 14). Episodes of elevated O_3 mixing ratios are observed at the national park ground stations, lagged by 1-2 days after the onset of Asian pollution events over the U.S. west coast discussed in Section 3 (gray shaded periods in Fig. 14). During these events from May-June 2010, surface O_3 anomalies of +15 ppbv are observed at the three sites, with the model attributing approximately 2-9 ppbv positive anomalies to Asian anthropogenic emissions. The GFDL AM3 high-resolution model captures 45-65% of observed day-to-day variability of surface O_3 at the ground stations, and the Asian anthropogenic enhancements can explain 25-30% of the variability in the model total O_3. The results indicate that subsiding Asian pollution directly contributes to some high-O_3 episodes at the CASTNet stations in the mountain west, consistent with our findings in Section 3 and Fig. 13.

6 Projecting Asian influences on U.S. surface ozone from space

In this section we give the first examples of a proposed space-based indicator for Asian pollution enhancements to surface O_3 over the western USA. The method

involves the correlation of daily AIRS CO columns at each 1°x1° grid box with the Asian contribution to MDA8 O_3 in the model surface layer for western U.S. national parks, for time lags of 0 to 3 days between the datasets. Figure 15 shows an example for Grand Canyon National Park. The time offset that gives the maximum correlation represents the transport time between the Asian pollution (represented by AIRS CO) arriving at the U.S. west coast and its influence on the surface receptor site. The region with the greatest correlation over the eastern North Pacific represents the region from which air is preferentially transported to the surface receptor site within the time lag indicated. In Fig. 15, strong correlations emerge with AIRS CO columns over approximately 30°- 50°N of the northeast Pacific; the region that gives the best correlation with the surface data shifts from west to east as the time offset decreases, reflecting the progression of Asian pollution towards the U.S. west coast. Correlation results for other ground stations in the western mountains show a similar large-scale feature, with the region experiencing the peak correlation falling within the boxes denoted in Fig. 15.

Based on the correlation analysis, we hypothesize that variability of AIRS CO measurements averaged over the eastern North Pacific within these boxes can serve at least as a qualitative warning index to inform regional air quality management decisions about incoming Asian enhancements to surface O_3 in the western mountains. Figure 16 elaborates on this hypothesis by illustrating a time series of AIRS CO averaged over the eastern North Pacific between 30°- 50°N latitudes and 145°-125°W longitudes (box in the lower-left panel of Fig. 15), together with Asian enhancements to surface MDA8 O_3 averaged over three selected CASTNet ground stations. The variability in AIRS CO is confounded by

the seasonal increase in OH, which leads to a decreasing trend (-6.1x10^{15} molecules/cm^2 per day, r^2=0.74) in CO from May to June. To highlight the CO variability due to trans-Pacific transport, we remove the linear trend from the time series of AIRS CO, which more clearly shows the three major trans-Pacific Asian pollution events discussed in Section 3 (May 7-12, May 17-22, and June 17-22). Further supporting the utility of satellite-based CO column measurements as an early warning indicator for surface air quality, we find that the timing of peak Asian enhancements on surface O_3 over the Rocky Mountains generally appears 1-2 days later than the peak AIRS CO over the eastern North Pacific.

Caution should be taken, however, that Asian pollution transported to the eastern North Pacific may not consistently reach the same locations given variability in meteorological conditions and storm structures. Future work should explore the interannual variability in the vertical extent of Asian pollution over the U.S. west coast as well as explore whether retrievals at particular levels (rather than the total column) contain a more quantitative relationship with the Asian surface O_3 over the U.S. Mountain West. The correlation between satellite-detected CO enhancements over the eastern North Pacific and the Asian influence reaching western U.S. surface air should be further examined using multiyear datasets.

7. Conclusions

We have applied a new high-resolution (~50x50 km^2) global chemistry-climate model (GFDL AM3) to examine the transport pathways of Asian pollution over the western U.S. in spring 2010, with a primary focus on the influence of Asian pollution to surface O_3 air quality. To the best of our knowledge, this is the first time a global high-resolution model with full stratospheric and tropospheric

chemistry has been employed to address the problem of trans-Pacific pollution transport.

Extensive observations during the CalNex field campaign (May-June 2010) enable a process-oriented assessment of the model in simulating regional transport and chemistry over the western USA. Evaluation with surface O_3 networks shows that the model captures much of the observed day-to-day variability in daily maximum 8-hour average O_3 (MDA8) in surface air, with correlation coefficients ranging from 0.4-0.8 and simulated standard deviations within 15% of those observed for most sites. The most severe limitation for our study is a high surface O_3 bias of 2-10 ppbv on average in the high elevation regions and up to 10-25 ppbv at the Pacific coastal sites (Section 4). The model bias in surface O_3 does not have a direct relationship with the Asian enhancement.

An integrated analysis of satellite measurements of CO and total O_3 column from AIRS, ozonesondes, and model diagnostics reveals two cases of interleaving and commingling of Asian pollution with stratospheric air associated with complex airstream interactions as mid-latitude cyclones cross the North American west coast during CalNex (May 17-20 and June 17-19) - a transport mechanism noted by prior studies [e.g. *Stohl and Trickl* 1999; *Cooper et al.*, 2004b]. The GFDL AM3 model successfully reproduces the prominent features of these events, and implies that transported stratospheric remnants from a deep tropopause fold may contribute 50-60% of distinct ozone layers between 2-4 km above the California coast. Asian pollution, which arrived one day after the deep tropopause fold, contributes 20-30% of total O_3 primarily located in the mid-troposphere when the

841 air was sampled by the ozonesondes (Section 3.1). We note our estimates
842 should be viewed as upper limits as discussed in Section 2.4.
843
844 Using both the model and observations, we further illustrate that Asian pollution
845 over the U.S. west coast descends isentropically behind cold fronts towards the
846 south (Sections 3.2-3.3), consistent with prior model studies [*Cooper et al*., 2011;
847 *Brown-Steiner and Hess* 2011]. Combined with the influence of additional O_3
848 produced from the thermal decomposition of Asian PAN during subsidence, the
849 Asian enhancement to O_3 at ~800 hPa exhibits a pronounced maximum in the
850 southwestern U.S. (including parts of California, Nevada, Utah, and Arizona;
851 Section 5.1). We find that the Asian enhancement in the model surface layer over
852 this region increases for total MDA8 O_3 concentrations in the 70-90 ppbv range
853 compared with that in the 60-70 ppbv range (Fig.13). We estimate that in the
854 absence of Asian anthropogenic emissions, 49% of springtime MDA8 O_3
855 exceedances of 70 ppbv in the model would not have occurred over the
856 southwestern U.S. For a 60 ppbv threshold, that statistic is 20% (Section 5.2).
857
858 During strong trans-Pacific transport events, the Asian enhancement to MDA8 O_3
859 in western U.S. surface air can reach 8-15 ppbv in high-elevation regions
860 experiencing peak surface O_3 levels in excess of 60 ppbv -- the lowest value
861 proposed for a ozone NAAQS reconsideration (Figs. 7 and 9). We further
862 demonstrate the potential for using near real-time satellite measurements of CO
863 columns (AIRS) over the eastern North Pacific at daily intervals to develop
864 space-based criteria to identify these strong Asian pollution events (Figs. 15 and
865 16). Such a space-based index could serve as an early-warning indicator (lead
866 time of 1-2 days) for the potential influence of Asian pollution to surface O_3 air

quality and any associated health advisories for National Park Services.

Our analysis suggests that consideration of enhancements from Asian anthropogenic emissions will be important to develop effective state implementation plans (and associated emission control strategies) for the western United States, particularly under more stringent NAAQS for O_3. Asian NO_x emissions are projected to increase up to ~50% from 2010-2050 in the RCP (Representative Concentration Pathways) scenarios for IPCC Fifth Assessment Report [*Moss et al*., 2010]. We thus expect that the Asian component of U.S. baseline ozone will continue to increase in the coming decades.

Acknowledgements:

This work is supported by the Cooperative Institute for Climate Science (CICS) -- a collaboration between Princeton University and NOAA Geophysical Fluid Dynamics Laboratory (GFDL). The satellite data analysis is funded by the NASA Air Quality Applied Science Team (AQAST) (NNH09ZDA001N). Funding for the IONS-2010 field campaign was provided by NOAA ESRL Health of the Atmosphere Program, NASA Tropospheric Chemistry Program, U. S. Navy, Environment Canada, and NOAA's National Air Quality Forecast Capability. We acknowledge the free use of tropospheric NO_2 column data from the SCIAMACHY sensor from www.tenis.nl and Bahreini Roya at NOAA ESRL for help collecting the AMS aerosol measurements onboard the WP-3D aircraft. We are grateful to Songmiao Fan and Hiram Levy II at NOAA GFDL and Pat Dolwick at EPA for helpful comments in improving an earlier version of this manuscript.

References:

Aumann, H. H., et al. (2003), AIRS/AMSU/HSB on the Aqua mission: Design, science objectives, data products, and processing systems, IEEE Trans. Geosci. Remote Sens., 41, 2, doi:10.1109/TGRS.2002.808356.

Austin, J., and R.J. Wilson (2006), Ensemble simulations of the decline and recovery of stratospheric ozone.J. Geophys. Res.,111, D16314, doi10.1029/2005JD006907.

Austin, J., and R.J. Wilson (2010), Sensitivity of polar ozone to sea surface temperatures and halogen amounts. J. Geophys. Res., 115, doi: 10.1029/2009JD013292.

Bahreini et al. (2010), Organic aerosol formation in urban and industrial plumes near Houston and Dallas, Texas, J. Geophys. Res., 114 (D00F16), doi:10.1029/2008JD011493

Bian, J., A. Gettelman, H. Chen, and L. L. Pan (2007), Validation of satellite ozone profile retrievals using Beijing ozonesonde data, J. Geophys. Res., 112, D06305, doi:10.1029/2006JD007502.

Boersma, K.F., H.J. Eskes and E.J. Brinksma (2004), Error Analysis for Tropospheric NO2 Retrieval from Space, J. Geophys. Res. 109 D04311, doi:10.1029/2003JD003962

Brock, C. A., et al. (2004), Particle characteristics following cloud-modified transport from Asia to North America, J. Geophys Res., 109, D23S26, doi:10.1029/2003JD004198

Brown-Steiner, B., and P. Hess (2011), Asian influence on surface ozone in the United States: a comparison of chemistry, seasonality, and transport mechanisms**,** J. Geophys. Res., *116*, D17309**,** doi:10.1029/2011JD015846

Burk, S. D., and W. T. Thompson (1996), The summertime low-level jet and marine boundary layer structure along the California coast. Mon. Wea. Rev., 124, 668–686.

Chen, Y., Zhao, C., Zhang, Q., Deng., Z., Huang, M., and Ma, X. (2009), Aircraft study of mountain chimney effect of Beijing, China, J. Geophys. Res., 114, D08306, doi:10.1029/2008JD010610

Chin, M., T. Diehl, P. Ginoux, and W. Malm (2007), Intercontinental transport of pollution and dust

aerosols: implications for regional air quality, Atmos. Chem. Phys., 7, 5501-5517

Cooper, O. R., et al. (2004a), A case study of transpacific warm conveyor belt transport: Influence of merging airstreams on trace gas import to North America, J. Geophys. Res., 109, D23S08, doi:10.1029/2003JD003624.

Cooper, O. R., et al. (2004b), On the life cycle of a stratospheric intrusion and its dispersion into polluted warm conveyor belts, J. Geophys. Res., 109, D23S09, doi:10.1029/2003JD004006.

Cooper, O. R., et al. (2010), Increasing springtime ozone mixing ratios in the free troposphere over western North America, Nature, 463, doi:10.1038/nature08708

Cooper, O. R, et al. (2011), Measurement of western U.S. baseline ozone from the surface to the tropopause and assessment of downwind impact regions, J. Geophys. Res., doi:10.1029/2011JD016095

Dentener, F., et al. (2006), Emissions of primary aerosol and precursor gases in the years 2000 and 1750 prescribed datasets for AeroCom, Atmos. Chem. Phys., 6, 4321-4344.

Divakarla, M., et al. (2008), Evaluation of Atmospheric Infrared Sounder ozone profiles and total ozone retrievals with matched ozonesonde measurements, ECMWF ozone data, and Ozone Monitoring Instrument retrievals, J. Geophys. Res., 113, D15308, doi:10.1029/2007JD009317.

Donner, L. J., Wyman, B. L., Hemler, R. S. et al (2011), The Dynamical Core, Physical Parameterizations, and Basic Simulation Characteristics of the Atmospheric Component AM3 of the GFDL Global Coupled Model CM3. Journal of Climate, 24, 3484–3519, doi: 10.1175/2011JCLI3955.1

Drewnick, F., et al. (2005), A new time-of-flight aerosol mass spectrometer (TOF-AMS)-Instrument description and first field deployment. Aerosol Sci. Technol., 39 (7), 637-658, doi: 10.1080/02786820500182040.

Dunlea, E. J., et al. (2009), Evolution of Asian aerosols during transpacific transport in INTEX-B, Atmos. Chem. Phys., 9, 7257-7287, doi:10.5194/acp-9-7257-2009

943 Edwards, D. P., et al. (2003), Tropospheric ozone over the tropical Atlantic: A satellite perspective,
944 J. Geophys. Res., 108(D8), 4237, doi:10.1029/2002JD002927.
945 Emmons, L.K., et al. (2010), Description and evaluation of the Model for Ozone and Related
946 chemical Tracers, version 4 (MOZART-4). Geosci. Model Dev., **3,** 43-67.
947 Esler, J. G., P. H. Haynes, K. S. Law, H. Barjat, K. Dewey, J. Kent, S. Schmitgen, and N.
948 Brough (2003), Transport and mixing between airmasses in cold frontal regions during
949 Dynamics and Chemistry of Frontal Zones (DCFZ), J. Geophys. Res., 108, 4142,
950 doi:10.1029/2001JD001494.
951 Federal Register (2010) National Ambient Air Quality Standards for Ozone, Vol. 75, No. 11, 2938-
952 3052, January 19, 2010
953 Felker, S. R., J. L. Moody, A. J. Wimmers, G. Osterman, and K. Bowman (2011), A multi-sensor
954 upper tropospheric ozone product (MUTOP) based on TES ozone and GOES water vapor:
955 derivation, Atmos. Chem. Phys., 11, 6515-6527.
956 Fiore, A. M., D. J. Jacob, I. Bey, R. M. Yantosca, B. D. Field, A. C. Fusco, and J. G.Wilkinson
957 (2002), Background ozone over the United States in summer: Origin, trend, and
958 contribution to pollution episodes, J. Geophys. Res.,107(D15), 4275,
959 10.1029/2001JD000982.
960 Goldstein, A. H., et al. (2004), Impact of Asian emissions on observations at Trinidad Head,
961 California, during ITCT 2K2, J. Geophys. Res., 109, D23S17, doi:10.1029/2003JD004406.
962 Golaz, Jean-Christophe, Marc Salzmann, Leo J. Donner, Larry W. Horowitz, Yi Ming, Ming Zhao
963 (2011), Sensitivity of the aerosol indirect effect to subgrid variability in the cloud
964 parameterization of the GFDL Atmosphere General Circulation Model AM3. Journal of
965 Climate, 24, 3145–3160, doi: 10.1175/2010JCLI3945.1
966 Griffies, Stephen M., Michael Winton, Leo J. Donner, et al (2011), GFDL's CM3 Coupled Climate
967 Model: Characteristics of the Ocean and Sea Ice Simulations. Journal of Climate, Journal
968 of Climate, 24, 3520–3544, doi: 10.1175/2011JCLI3964.1

969 Guenther, A., T. Karl, P. Harley, C. Wiedinmyer, P. Palmer, and C. Geron (2006), Estimates of
970 global terrestrial isoprene emissions using MEGAN (Model of Emissions of Gases and
971 Aerosols from Nature), Atmos. Chem Phys., 6, 3181-3210.
972 Heald, C.L., D.J. Jacob, A.M. Fiore et al (2003), Asian outflow and transpacific transport of carbon
973 monoxide and ozone pollution: An integrated satellite, aircraft and model perspective, J.
974 Geophys. Res., 108 (D24), 4804, doi:10.1029/2003JD003507, 2003
975 Holloway, J., R. Jakoubek, D. Parrish, C. Gerbig, A. Volz-Thomas, S. Schmitgen, A. Fried, B.
976 Wert, B. Henry, and J. Drummond (2000), Airborne intercomparison of vacuum ultraviolet
977 fluorescence and tunable diode laser absorption measurements of tropospheric carbon
978 monoxide, J. Geophys. Res., 105(D19), 24251-24261.
979 Horowitz, L.W., S. Walters, and D. Mauzerall et al (2003), A global simulation of tropospheric
980 ozone and related tracers: description and evaluation of MOZART, version 2. J. Geophys.
981 Res., 108, D24, doi.10.1029/2002JD002853.
982 Huang, M., et al. (2010), Impacts of transported background ozone on California air quality during
983 845 the ARCTAS-CARB period a multi-scale modeling study, Atmos. Chem. Phys., 10,
984 6947-6968.
985 Hudman, R. C., et al. (2004), Ozone production in transpacific Asian pollution plumes and
986 implications for ozone air quality in California, J. Geophys. Res., 109,
987 D23S10,10.1029/2004JD004974
988 Jacob, D. J., J. A. Logan, and P. P. Murti (1999), Effect of rising Asian emissions on surface
989 ozone in the United States, Geophys. Res. Lett., 26, 2175–2178,
990 Jaeglé, L., D. A. Jaffe, H. U. Price, P. Weiss-Penzias, P. I. Palmer, M. J. Evans, D. J. Jacob, and I.
991 Bey (2003), Sources and budgets for CO and O3 in the northeastern Pacific during the
992 spring of 2001: Results from the PHOBEA-II Experiment, J. Geophys. Res., 108(D20),
993 8802, doi:10.1029/2002JD003121.
994 Jaffe, D., et al. (1999), Transport of Asian air pollution to North America, Geophys. Res. Lett.,

995 26(6), 711-714.
996 Jaffe D.A., Parrish D., Goldstein A., Price H., and Harris J. (2003), Increasing background ozone
997 during spring on the west coast of North America. Geophys.Res Letts. Vol. 30, No. 12,
998 1613, doi: 10.1029/2003GL017024.
999 Kanamitsu, M., Alpert, J., Campana, K., Caplan, P., Deaven, D., Iredell, M., Katz, B., Pan, H.-L.,
1000 Sela, J., and White, G. (1991), Recent changes implemented into the global forecast
1001 system at NMC, Weather Forecast., 6, 425–435
1002 Keating, T. J., West, J. J. & Farrell, A. E. (2004) in Intercontinental Transport of Air Pollution, ed.
1003 Stohl, A. (Springer, Berlin), pp. 295–320
1004 Kleinman, L. et al. (1994), Ozone formation at a rural site in the southeastern United States, J.
1005 Geophys. Res., 99, D2, doi:10.1029/93JD02991, 1994
1006 Knutson, Thomas R., Joseph J Sirutis, Stephen T Garner, Gabriel A Vecchi, and Isaac Held
1007 (2008), Simulated reduction in Atlantic hurricane frequency under twenty-first-century
1008 warming conditions. Nature Geoscience, 1(6), 359-364.
1009 Koumoutsaris S., I. Bey, S. Generoso, and V. Thouret (2008), Influence of El Nino-Southern
1010 Oscillation on the interannual variability of tropospheric ozone in the northern mid-latitudes,
1011 J. Geophys. Res., 113, D19301, doi:10.1029/2007JD00975.
1012 Lamarque, J.-F., et al. (2010), Historical (1850–2000) gridded anthropogenic and biomass
1013 burning emissions of reactive gases and aerosols: methodology and application, Atmos.
1014 Chem. Phys.,10, 7017–7039
1015 Lamsal, L. N., R. V. Martin, A. Padmanabhan, A. van Donkelaar, Q. Zhang, C. E. Sioris, K.
1016 Chance, T. P. Kurosu, and M. J. Newchurch (2011), Application of satellite observations for
1017 timely updates to global anthropogenic NOx emission inventories, Geophys. Res. Lett., 38,
1018 L05810, doi:10.1029/2010GL046476.
1019 Langford, A. O., C. J. Senff, R. J. Alvarez, R. M. Banta, and R. M. Hardesty (2010), Long-range
1020 transport of ozone from the Los Angeles Basin: A case study, Geophys. Res. Lett., 37,

L06807, doi:10.1029/2010GL042507.

Lei, Y., Zhang, Q., He, K. B., and Streets, D. G. (2010), Primary aerosol emission trends for China, 1990–2005, Atmos. Chem. Phys. Discuss., 10, 17153-17212, doi:10.5194/acpd-10-17153-2010

Li, F., P. Ginoux, and V. Ramaswamy (2010) Transport of Patagonian dust to Antarctica, J. Geophys. Res., 115, D18217, doi:10.1029/2009JD012356.

Lin, J.-T. and McElroy, M. B. (2011) Detection from space of a reduction in anthropogenic emissions of nitrogen oxides during the Chinese economic downturn, Atmos. Chem. Phys. Discuss., 11, 193-223, doi:10.5194/acpd-11-193-2011

Lin, M., T. Holloway, T. Oki, D.G. Streets, and A. Richter (2009), Multi-scale model analysis of boundary layer ozone over East Asia. Atmos. Chem. and Phys., 9, 3277-3301

Lin, M., Holloway, T., Carmichael, G. R., and Fiore, A. M. (2010), Quantifying pollution inflow and outflow over East Asia in spring with regional and global models. Atmos. Chem. Phys., 10, 4221-4239

Lu, Z., Streets, D. G., Zhang, Q., Wang, S., Carmichael, G. R., Cheng, Y. F., Wei, C., Chin, M., Diehl, T., and Tan, Q. (2010), Sulfur dioxide emissions in China and sulfur trends in East Asia since 2000, Atmos. Chem. Phys., 10, 6311-6331, doi:10.5194/acp-10-6311-2010

McMillan, W. W., et al. (2005), Daily global maps of carbon monoxide from NASA's Atmospheric Infrared Sounder, Geophys. Res. Lett., 32, L11801, doi:10.1029/2004GL021821.

McMillan, W. W., J. X. Warner, M. McCourt Comer, E. Maddy, A. Chu, L. Sparling, E. Eloranta, R. Hoff, G. Sachse, and C. Barnet (2008), AIRS views transport from 12 to 22 July 2004 Alaskan/Canadian fires: Correlation of AIRS CO and MODIS AOD with forward trajectories and comparison of AIRS CO retrievals with DC-8 in situ measurements during INTEX-A/ICARTT, J Geophys Res, 113, D20301, doi:10.1029/2007JD009711.

McMillan, W. W.; Evans, K. D.; Barnet, C. D.; Maddy, E. S.; Sachse, G. W.; Diskin, G. S. (2011), Validating the AIRS Version 5 CO Retrieval With DACOM In Situ Measurements

During INTEX-A and -B, Geoscience and Remote Sensing, IEEE Transactions, 49 (7), 2802 - 2813, doi:10.1109/TGRS.2011.2106505

Monahan, K. P., L. L. Pan, A. J. McDonald, G. E. Bodeker, J. Wei, S. E., George, C. D. Barnet, and E. Maddy (2007), Validation of AIRS v4 ozone profiles in the UTLS using ozonesondes from Lauder, NZ and Boulder, USA, J. Geophys. Res., 112, D17304, doi:10.1029/2006JD008181.

Moss, R. H., et al (2010), The next generation of scenarios for climate change research and assessment, Nature 463, 747-756, doi:10.1038/nature08823

Moxim, W., H. Levy II, and P. Kasibhatla (1996), Simulated global tropospheric PAN: Its transport and impact on NOx, J. Geophys. Res., 101(D7), 12621-12638.

Ohara, T., Akimoto, H., Kurokawa, J., Horii, N., Yamaji, K., Yan, X., and Hayasaka, T. (2007) An Asian emission inventory of anthropogenic emission sources for the period 1980–2020, Atmos. Chem. Phys., 7, 4419-4444, doi:10.5194/acp-7-4419-2007

Oltmans, S. J., Lefohn, A. S., Harris, J. M., and Shadwick, D. S. (2008), Background ozone levels of air entering the west coast of the U.S. and assessment of longer-term changes, Atmos. Environ., 42, 6020–6038.

Parish, T. R. (2000), Forcing of the Summertime Low-Level Jet along the California Coast. J. Appl. Meteor., 39, 2421–2433

Parrish, D., J. Holloway, R. Jakoubek, M. Trainer, T. Ryerson, G. Hübler, F. Fehsenfeld, J. Moody, and O. Cooper (2000), Mixing of anthropogenic pollution with stratospheric ozone: A case study from the North Atlantic wintertime troposphere, J. Geophys. Res., 105(D19), 24363-24374.

Parrish, D. D., D.B. Millet, A.H. Goldstein (2009), Increasing ozone in marine boundary layer inflow at the west coasts of North America and Europe, Atmos. Chem. Phys. 9, 1303-1323.

Parrish, D. D., Aikin, K. C., Oltmans, S. J., Johnson, B. J., Ives, M., and Sweeny, C. (2010), Impact of transported background ozone inflow on summertime air quality in a California

1073 ozone exceedance area, Atmos. Chem. Phys., 10, 10093-10109, doi:10.5194/acp-10-
1074 10093-2010
1075 Pan, L. L., et al. (2007), Chemical behavior of the tropopause observed during the Stratosphere-
1076 Troposphere Analyses of Regional Transport (START) experiment, J. Geophys. Res., 112,
1077 D18110, doi:10.1029/2007JD008645.
1078 Peltier, R. E., Hecobian, A. H., Weber, R. J., Stohl, A., Atlas, E. L., Riemer, D. D., Blake, D. R.,
1079 Apel, E., Campos, T., and Karl, T. (2008), Investigating the sources and atmospheric
1080 processing of fine particles from Asia and the Northwestern United States measured during
1081 INTEX B, Atmos. Chem. Phys., 8, 1835–1853
1082 Pfister, G. G., Parrish, D. D., Worden, H., Emmons, L. K., Edwards, D. P., Wiedinmyer, C., Diskin,
1083 G. S., Huey, G., Oltmans, S. J., Thouret, V., Weinheimer, A., and Wisthaler, A. (2011),
1084 Characterizing summertime chemical boundary conditions for airmasses entering the US
1085 West Coast, Atmos. Chem. Phys., 11, 1769-1790, doi:10.5194/acp-11-1769-2011
1086 Pittman, J. V., et al. (2009), Evaluation of AIRS, IASI, and OMI ozone profile retrievals in the
1087 extratropical tropopause region using in situ aircraft measurements,J. Geophys. Res., 114,
1088 D24109, doi:10.1029/2009JD012493.
1089 Putman, W. M. and S.-J. Lin (2007), Finite-volume transport on various cubed-sphere grid. J.
1090 Comput. Phys., 227, 5578.
1091 Rasmussen, D.J., A.M. Fiore, V. Naik, L.W. Horowitz, S.J. McGinnis, and M.G. Schultz
1092 (2011), Surface ozone-temperature relationships in the eastern US: A monthly climatology
1093 for evaluating chemistry-climate models. Atmos. Environ., submitted.
1094 Rastigejev, Y., R. Park, M.P. Brenner, and D.J. Jacob (2010), Resolving intercontinental pollution
1095 plumes in global models of atmospheric transport ,J. Geophys. Res., 115, D02302
1096 Reidmiller, D R., and A. M Fiore, et al. (2009), The influence of foreign vs. North American
1097 emissions on surface ozone in the US**.** Atmospheric Chemistry and Physics**,** 9**,** 5027-5042.
1098 Richter, A., et al. (2005), Increase in tropospheric nitrogen dioxide over China observed from

space, Nature, 437(7055), 129– 132, doi:10.1038/nature04092.

Ryerson, T., et al. (1998), Emissions lifetimes and ozone formation in power plant plumes, J. Geophys. Res., 103(D17), 22569-22583

Skamarock William C., Joseph B. Klemp, Jimy Dudhia, David O. Gill, Dale M. Barker, Michael G. Duda, Xiang-Yu Huang, Wei Wang, Jordan G. Powers (2008), A Description of the Advanced Research WRF Version 3, NCAR TECHNICAL NOTE, NCAR/TN–475+STR

Susskind, J., C. D. Barnet, and J. M. Blaisdell (2003), Retrieval of atmospheric and surface parameters from AIRS/AMSU/HSB data in the presence of clouds, IEEE Trans. Geosci. Remote Sens., 41, 390–409

Stohl, A., and T. Trickl (1999), A textbook example of long-range transport: Simultaneous observation of ozone maxima of stratospheric and North American origin in the free troposphere over Europe, J. Geophys. Res., 104, 30,445– 30,462

Stohl, A., et al. (2007), Arctic smoke record air pollution levels in the European Arctic during a period of abnormal warmth, due to agricultural fires in eastern Europe, Atmos. Chem. Phys., 7, 511–534

Tanimoto, H., Y. Sawa, H. Matsueda, I. Uno, T. Ohara, K. Yamaji, J. Kurokawa, and S. Yonemura (2005), Significant latitudinal gradient in the surface ozone spring maximum over East Asia, Geophys. Res. Lett., 32, L21805, doi:10.1029/2005GL023514

Task Force on Hemispheric Transport of Air Pollution (2010), Hemispheric Transport of Air Pollution 2010 , Part A: Ozone and Particulate Matter, United Nations, Air Pollution Studies No. 17.

Trainer, M. et al (1993), Correlations of ozone with NOx in photochemically aged air, J. Geophys. Res., 98, 2917-2925

Uno I, et al. (2009), Asian dust transported one full circuit around the globe. Nature Geoscience 2, 557 - 560, doi:10.1038/ngeo583.

Voulgarakis, A., P. J. Telford, A. M. Aghedo, P. Braesicke, G. Faluvegi, N. L. Abraham, K. W.

1125 Bowman, J. A. Pyle, and D. T. Shindell (2011), Global multi-year O3-CO correlation
1126 patterns from models and TES satellite observations, Atmospheric Chemistry and Physics,
1127 11, 5819–5838, 2011, doi:10.5194/acp-11-5819-2011
1128 Van Noije, T., Eskes, H., van Weele, M., and van Velthoven, P. (2004), Implications of the
1129 enhanced Brewer-Dobson circulation in European Centre for Medium-Range Weather
1130 Forecasts reanalysis ERA-40 for the stratosphere-troposphere exchange of ozone in global
1131 chemistry transport models, J. Geophys. Res., 109, D19308, doi:10.1029/2004JD004586
1132 Warner, Juying, M. McCourt Comer, C. D. Barnet, W. W. McMillan, W. Wolf, E. Maddy, and G.
1133 Sachse (2007), A comparison of satellite tropospheric carbon monoxide measurements
1134 from AIRS and MOPITT during INTEX-A, J Geophys Res, 112, D12S17,
1135 doi:10.1029/2006JD007925.
1136 Wei, J. C., et al. (2010), Ozone Profile Retrieval from an Advanced Infrared Sounder:
1137 Experiments withTropopause-Based Climatology and Optimal Estimation Approach,
1138 Journal of Atmospheric and Oceanic Technology, 27, 1123-1139, DOI:
1139 10.1175/2010JTECHA1384.1
1140 Wiedinmyer, C., Akagi, S. K., Yokelson, R. J., Emmons, L. K., Al-Saadi, J. A., Orlando, J. J., and
1141 Soja, A. J. (2011), The Fire INventory from NCAR (FINN): a high resolution global model to
1142 estimate the emissions from open burning, Geosci. Model Dev., 4, 625-641,
1143 doi:10.5194/gmd-4-625-2011
1144 Wimmers, A. J., J. L. Moody, E. V. Browell, J. W. Hair, W. B. Grant, C. F. Butler, M.A. Fenn, C. C.
1145 Schmidt, J. Li, and B. A. Ridley (2003), Signatures of tropopause folding in satellite imagery,
1146 J. Geophys. Res., 108(D4), 8360, doi:10.1029/2001JD001358.
1147 Wu, S., B. N. Duncan, D. J. Jacob, A. M. Fiore, and O. Wild (2009), Chemical nonlinearities in
1148 relating intercontinental ozone pollution to anthropogenic emissions, Geophys. Res.
1149 Lett., 36, L05806, doi:10.1029/2008GL036607
1150 Yienger, J., Galanter, M., Holloway, T., Phandis, M., Guttikunda, S., Carmichael, G., Moxim, W.,

1151 and Levy II, H. (2000), The episodic nature of air pollution transport from Asia to North
1152 America, J. Geophys. Res., 105(D22), 26 931–26 945
1153 Zhang, L., et al. (2006), Ozone-CO correlations determined by the TES satellite instrument in
1154 continental outflow regions, Geophys. Res. Lett., 33, L18804, doi:10.1029/2006GL026399.
1155 Zhang, L., D. J. Jacob, K. F. Boersma, et al. (2008), Transpacific transport of ozone pollution and
1156 the effect of recent Asian emission increases on air quality in North America: an integrated
1157 analysis using satellite, aircraft, ozonesonde, and surface observations, Atmos. Chem.
1158 Phys., 8, 6117-6136
1159 Zhang, L., D. J. Jacob, M. Kopacz, D. K. Henze, K. Singh, and D. A. Jaffe (2009), Intercontinental
1160 source attribution of ozone pollution at western U.S. sites using an adjoint method,
1161 Geophys. Res. Lett., 36, L11810.
1162 Zhang, L., et al. (2011), Improved estimate of the policy-relevant background ozone in the United
1163 States using the GEOS-Chem global model with $1/2^{o}$x$2/3^{o}$ horizontal resolution over North
1164 America, Atmospheric Environment, doi:10.1016/j.atmosenv.2011.07.054
1165 Zhang, Q., et al. (2009), Asian emissions in 2006 for the NASA INTEX-B mission, Atmos. Chem.
1166 Phys., 9, 5131-5153, doi:10.5194/acp-9-5131-2009

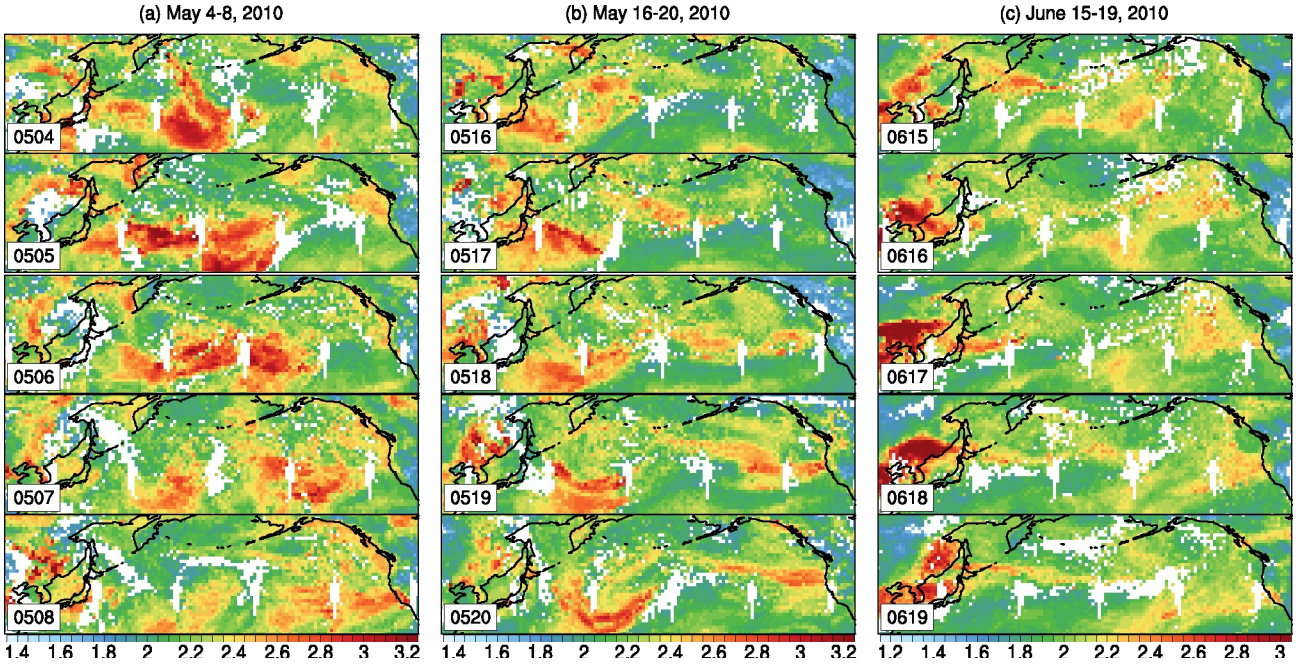

Figure 1. Major trans-Pacific Asian pollution events in May-June 2010 as seen from AIRS retrievals of CO total columns (10^{18} molecules cm^{-2}, Level 3 daily 1°x1° gridded products). Day and nighttime retrievals are combined, with white areas indicating no retrievals. Data bins are reordered so that neighboring gridded cells of data at the international dateline are no more than a swath of time apart (about 90 minutes).

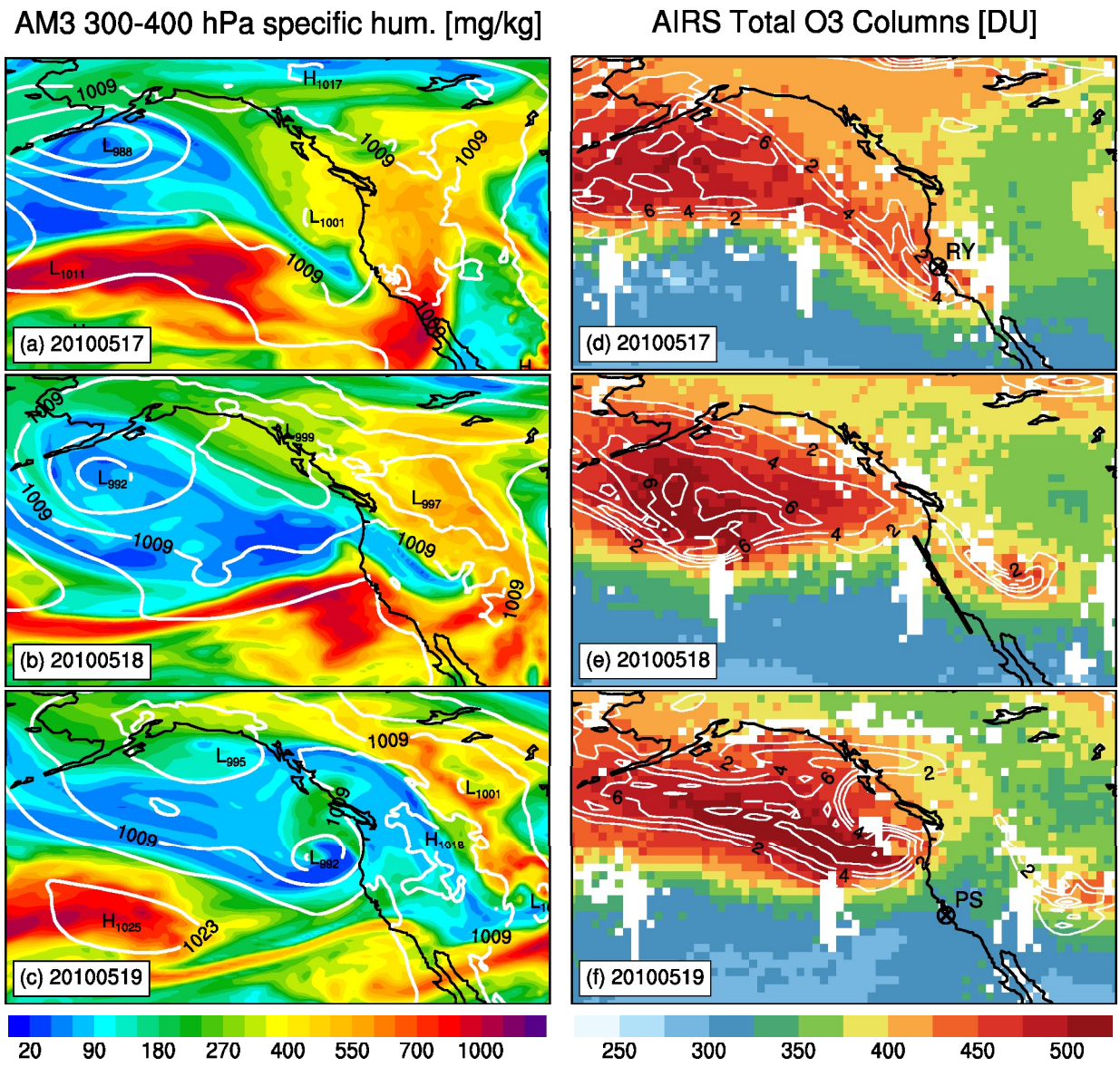

Figure 2. Evolution of two mid-latitude cyclones and associated flow structures over the Pacific North America on May 17-19, 2010. Shown are (left) AM3 6-hour mean sea level pressure (contours, hPa) with 300-400 hPa layer average specific humidity (shading, mg/kg) at 21:00 UTC and (right) AIRS retrievals of daily mean total column amounts of ozone (shading, DU) with 300 hPa potential vorticity (contours, PVU) computed from GFS Final analysis at 18:00 UTC. Only PV values greater than 2 PVU are contoured and signify air of essentially stratospheric origin. The thick black line along the California coast in (e) indicates the location of vertical cross-section shown in Figure 4.

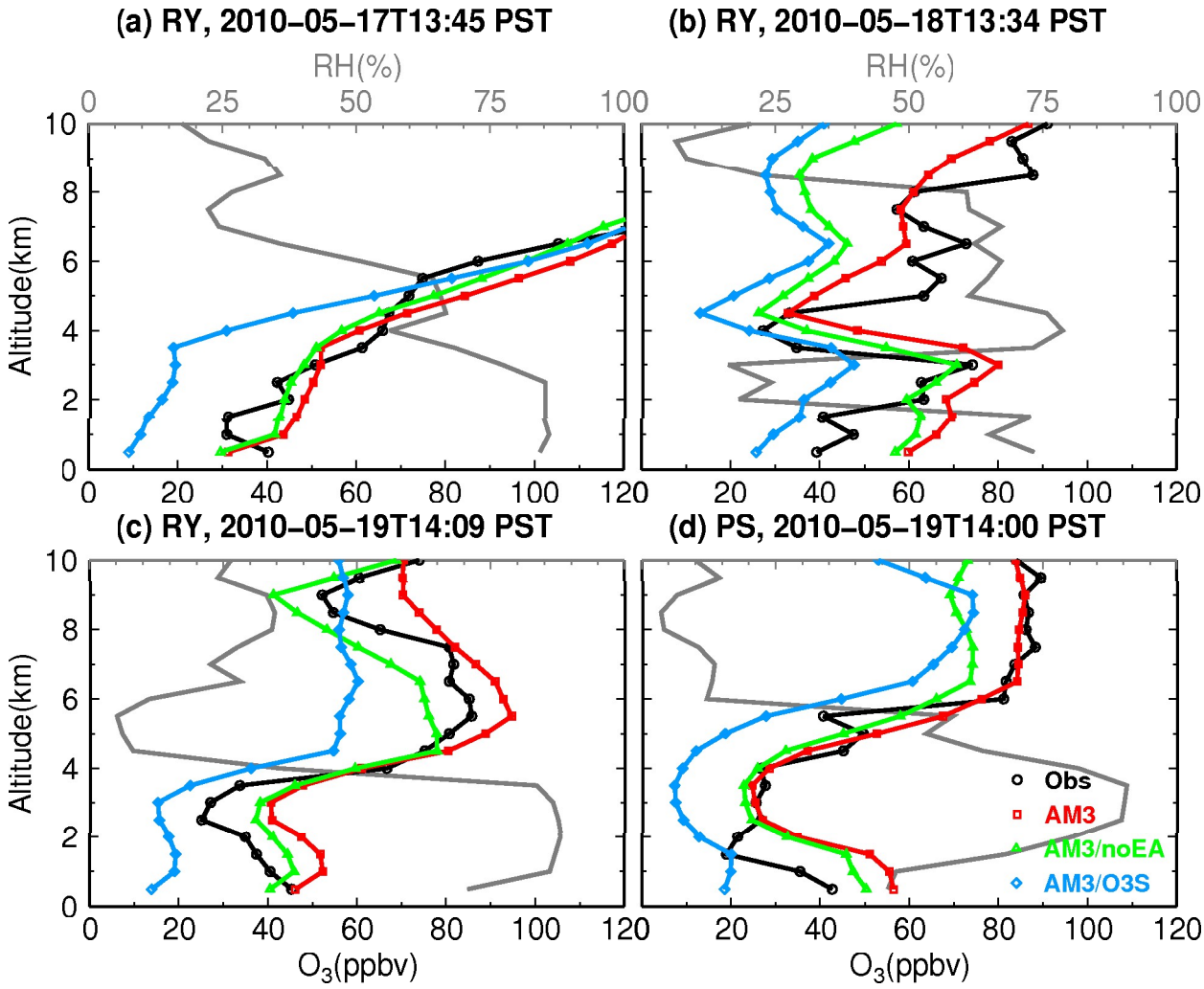

Figure 3. Observed vertical profiles of relative humidity (gray) and ozone (black) at Point Reyes (RY) and Point Sur (PS) sondes on May 17-19, together with model total ozone (red), stratospheric ozone tracer (blue), and model ozone from a sensitivity simulation with Asian anthropogenic emissions shut off (green). Model results have been interpolated to the sonde pressure and into 0.5-km altitude bins.

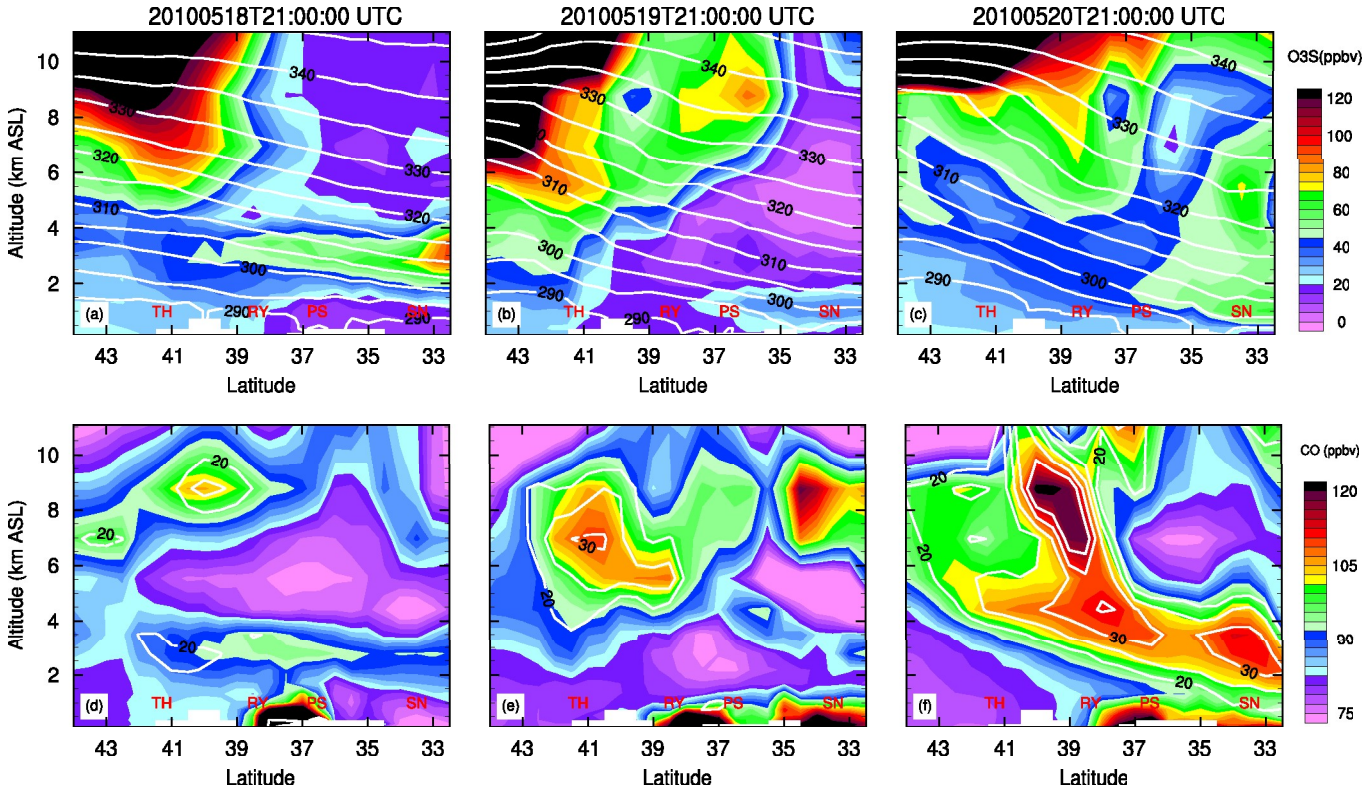

Figure 4. Vertical cross-section (thick black line in Fig.2e) illustrating the mixing between Asian pollution and stratospheric air on May 18-20, 2010. Shown are (top) AM3 stratospheric ozone tracer (shading, Section 2.3) with isentropic surfaces (contours, K) and (bottom) total CO (shading, ppbv) with Asian CO (contours, ppbv) as determined by the difference between the standard simulation and a sensitivity simulation with Asian anthropogenic emissions shut off. Letters in red denote locations of ozonesondes (Fig. S1).

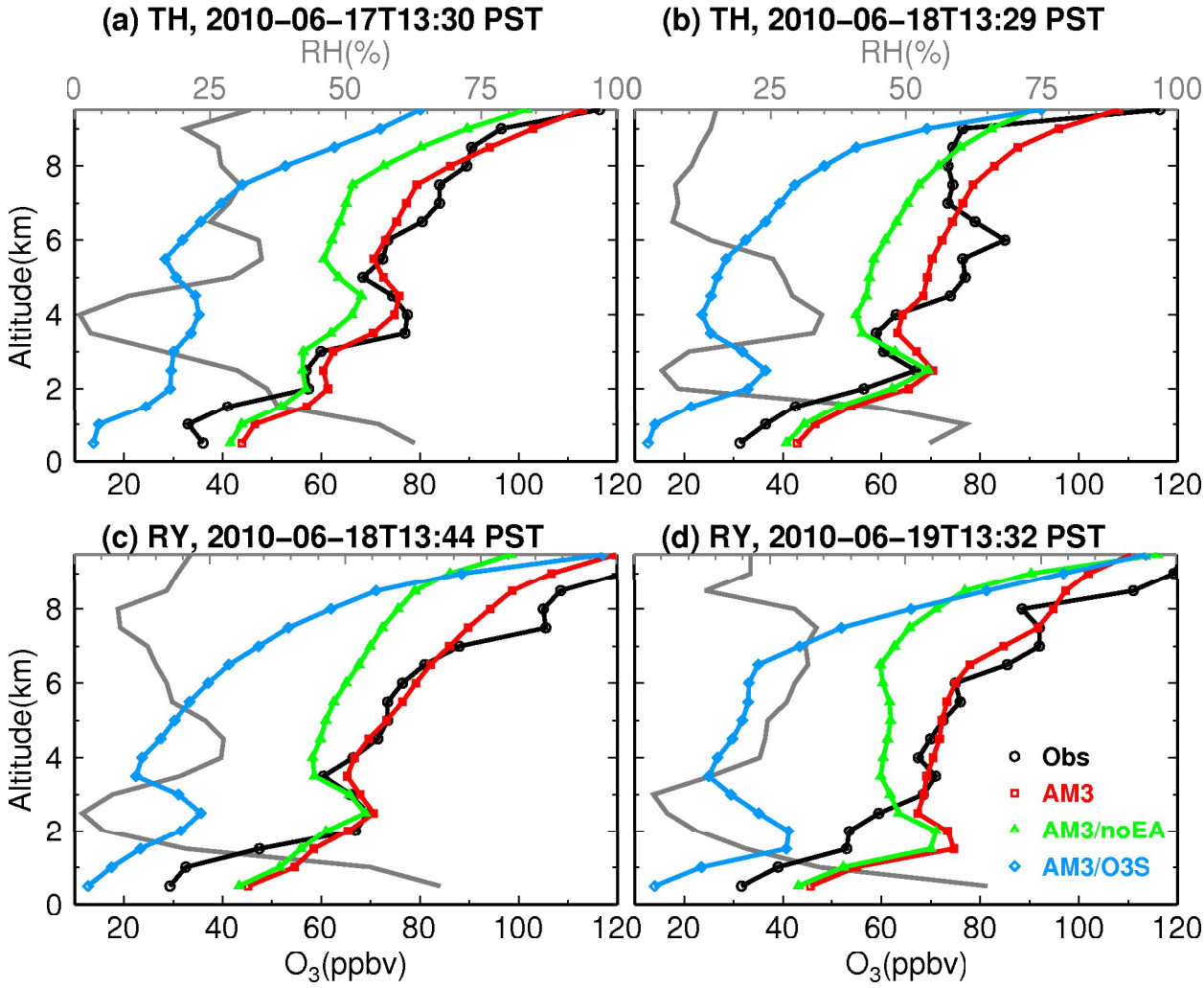

Figure 5. As in Figure 3, but for vertical profiles above Trinidad Head (TH) and Point Reyes (RY) on June 17-19, 2010.

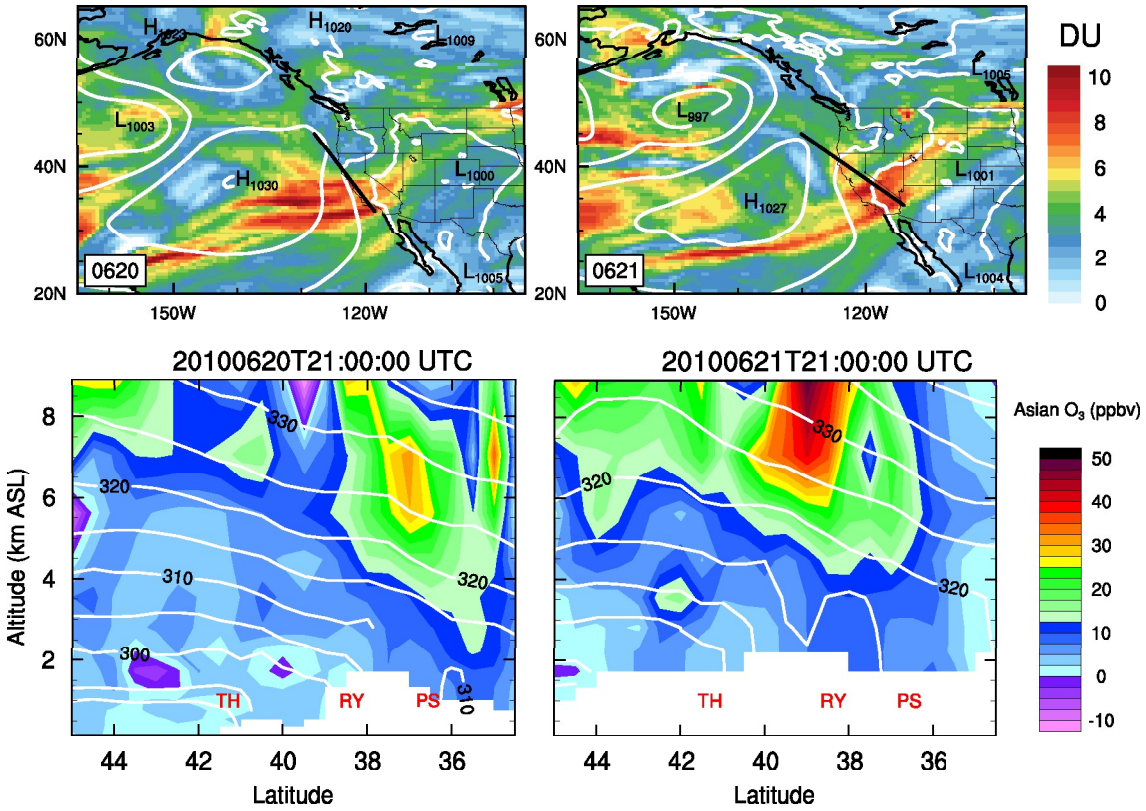

Figure 6. Propagation of Asian pollution from the North Pacific Ocean to the western USA from June 20-21, 2010. Shown are (top) Asian enhancements to daily mean tropospheric column ozone (shading) with sea level pressure (contours, hPa) and (bottom) subsidence of Asian ozone (shading) along isentropic surfaces (contours, K) as air masses travel from north to south (thick black lines in the top panels)

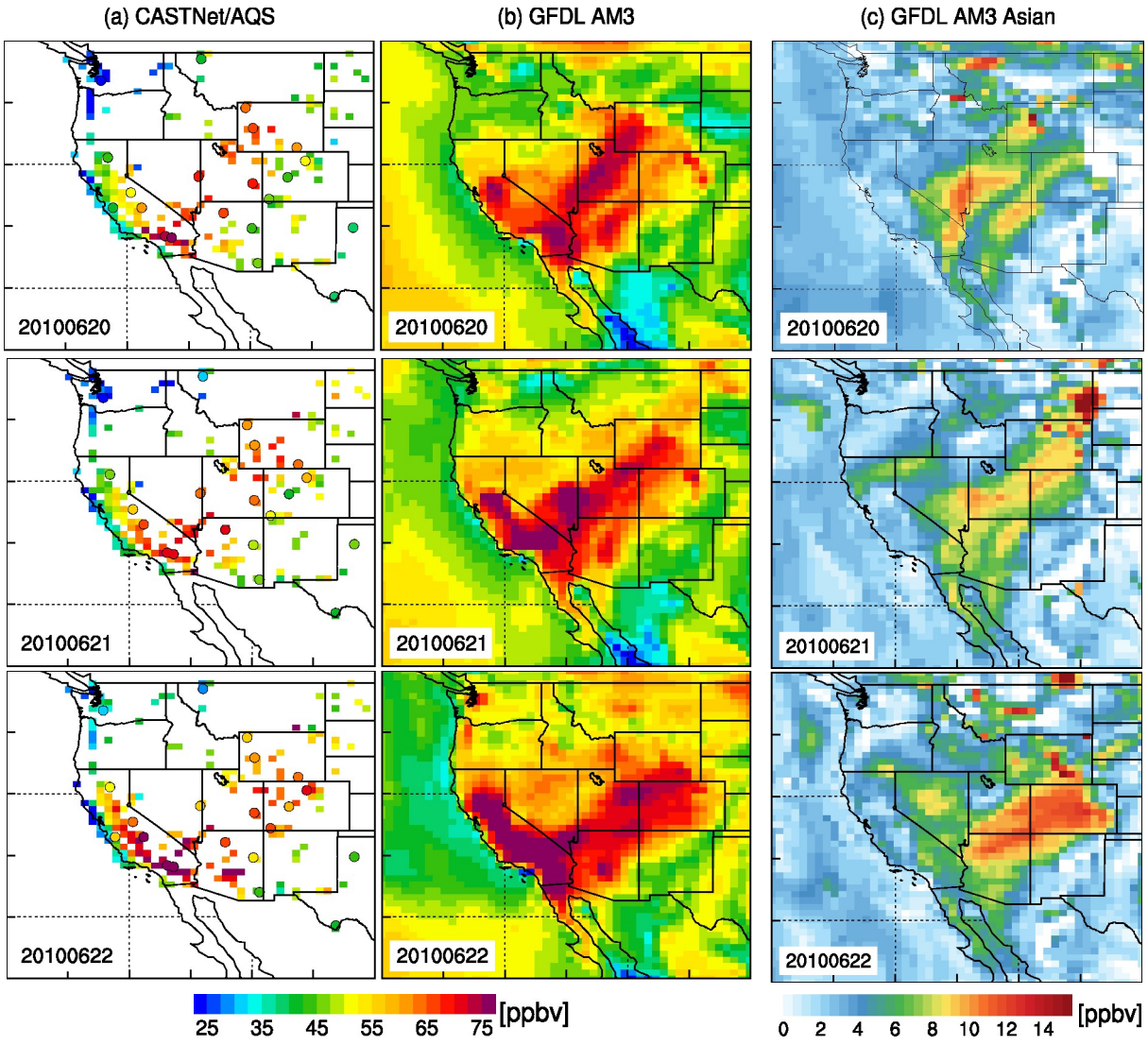

Figure 7. Spatial patterns of daily maximum 8-hour average ozone in western US surface air on June 20-22, 2010, showing (a) CASTNet (circles) and AQS (squares) observations, (b) results from the surface layer in the GFDL AM3 model, (c) the enhancements due to Asian anthropogenic emissions, estimated with AM3.

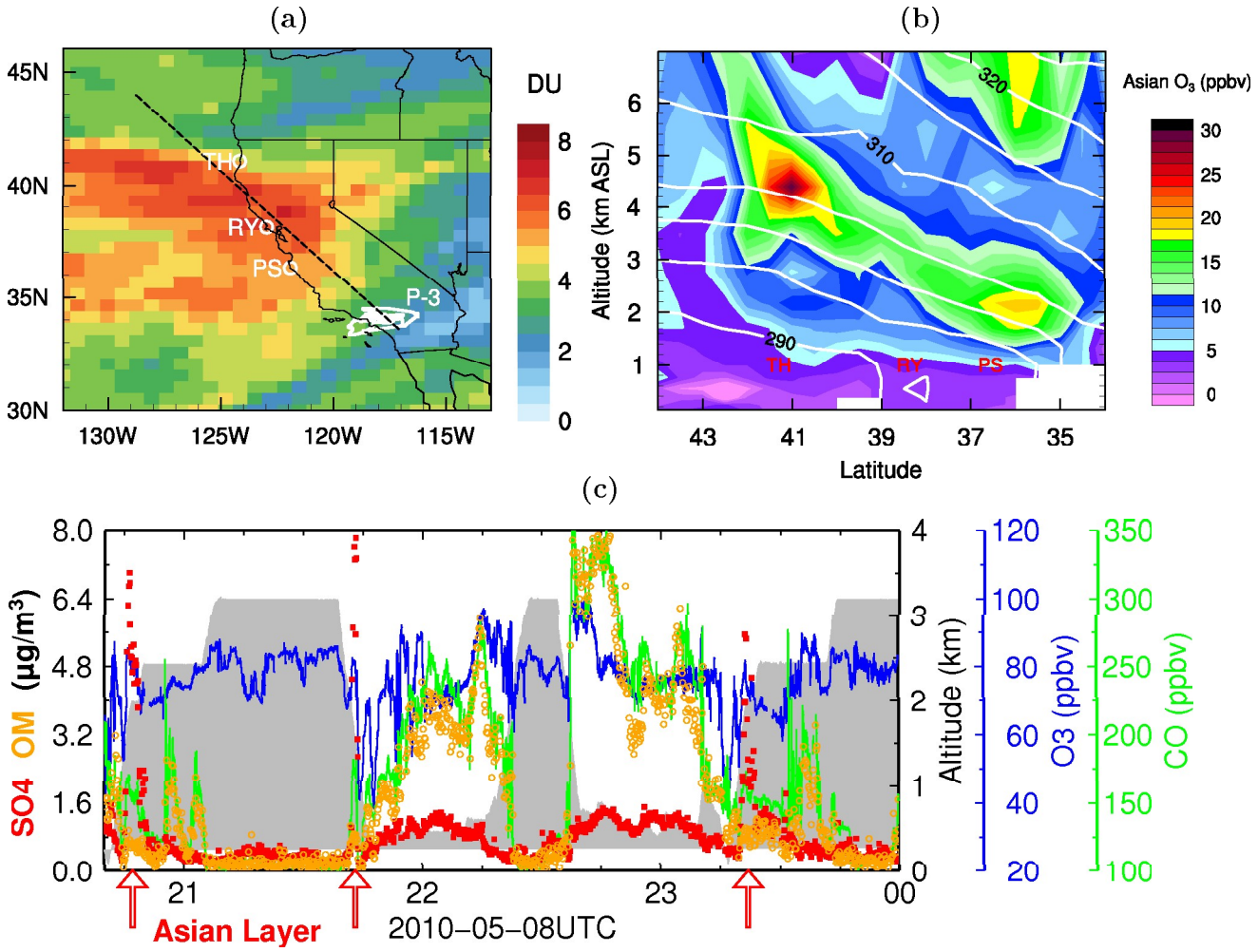

Figure 8. Transport of Asian pollutants to the lower troposphere of southern California on May 8, 2010. (a) Model Asian enhancements to the tropospheric column ozone. The dashed black line denotes the location of the ozone vertical cross-section shown in (b). The white line indicates the NOAA WP-3D flight path. (b) Model vertical distribution of Asian ozone (shading) with isentropic surfaces (contours, K) along the California coast. (c) Observed distributions of CO (green), O_3 (blue), sulfate (red) and organic aerosols (orange) along the WP-3D flight path, with altitude shown as gray shading.

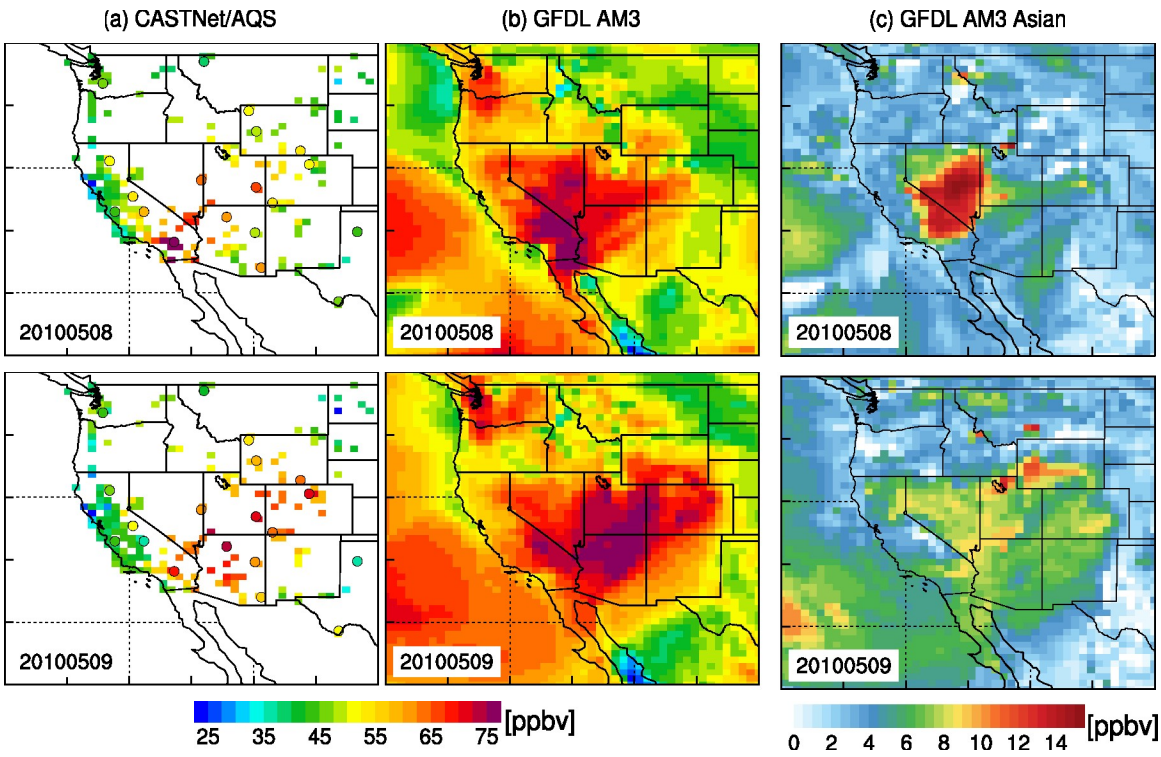

Figure 9. As in Figure 7, but for May 8-9, 2010.

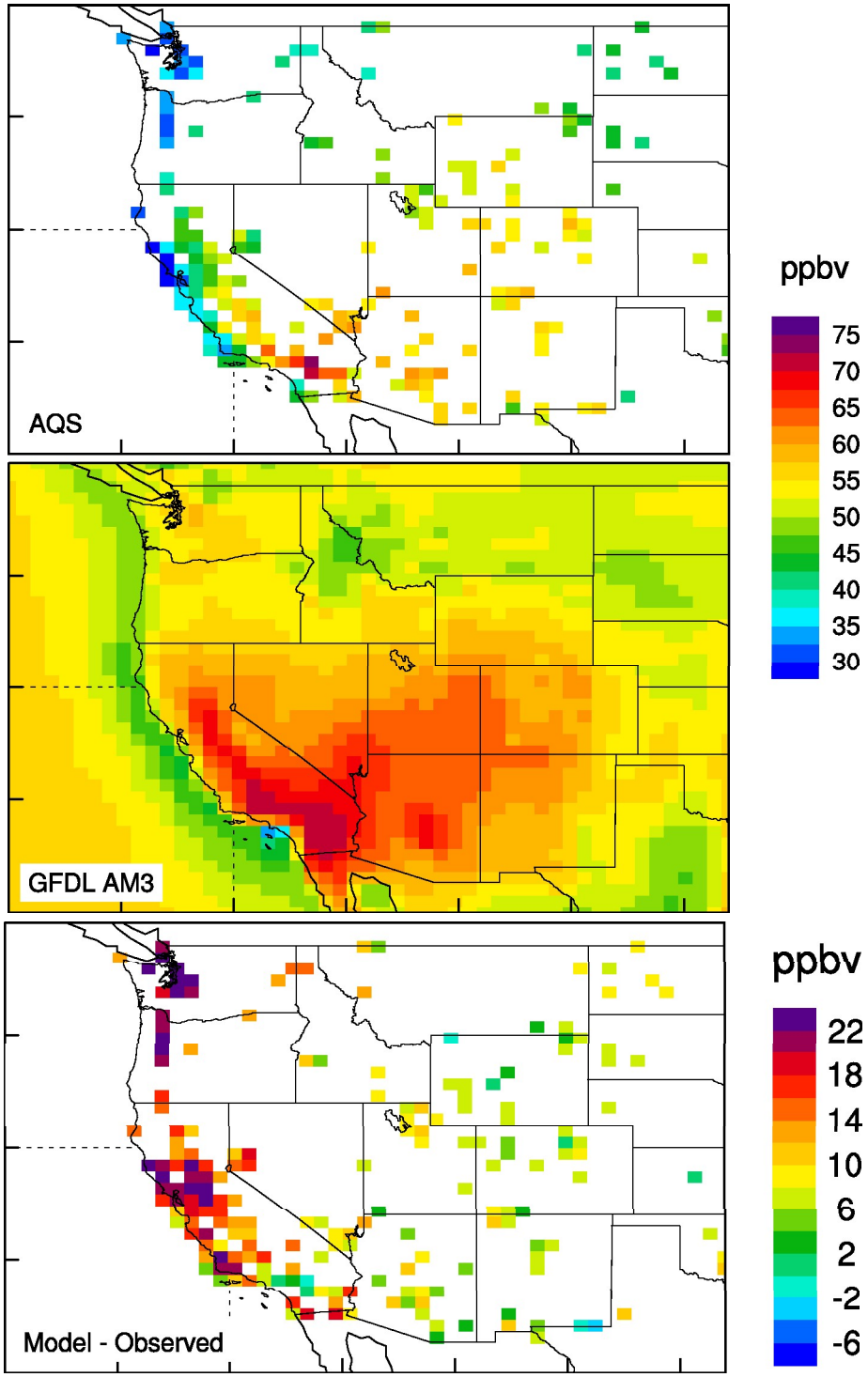

Figure 10. Mean daily maximum 8-hour average ozone mixing ratios in surface air over the western U.S. in May-June 2010 showing (top) the AQS observations, (middle) the GFDL AM3 model surface layer, and (bottom) the difference between the AM3 model and AQS observations.

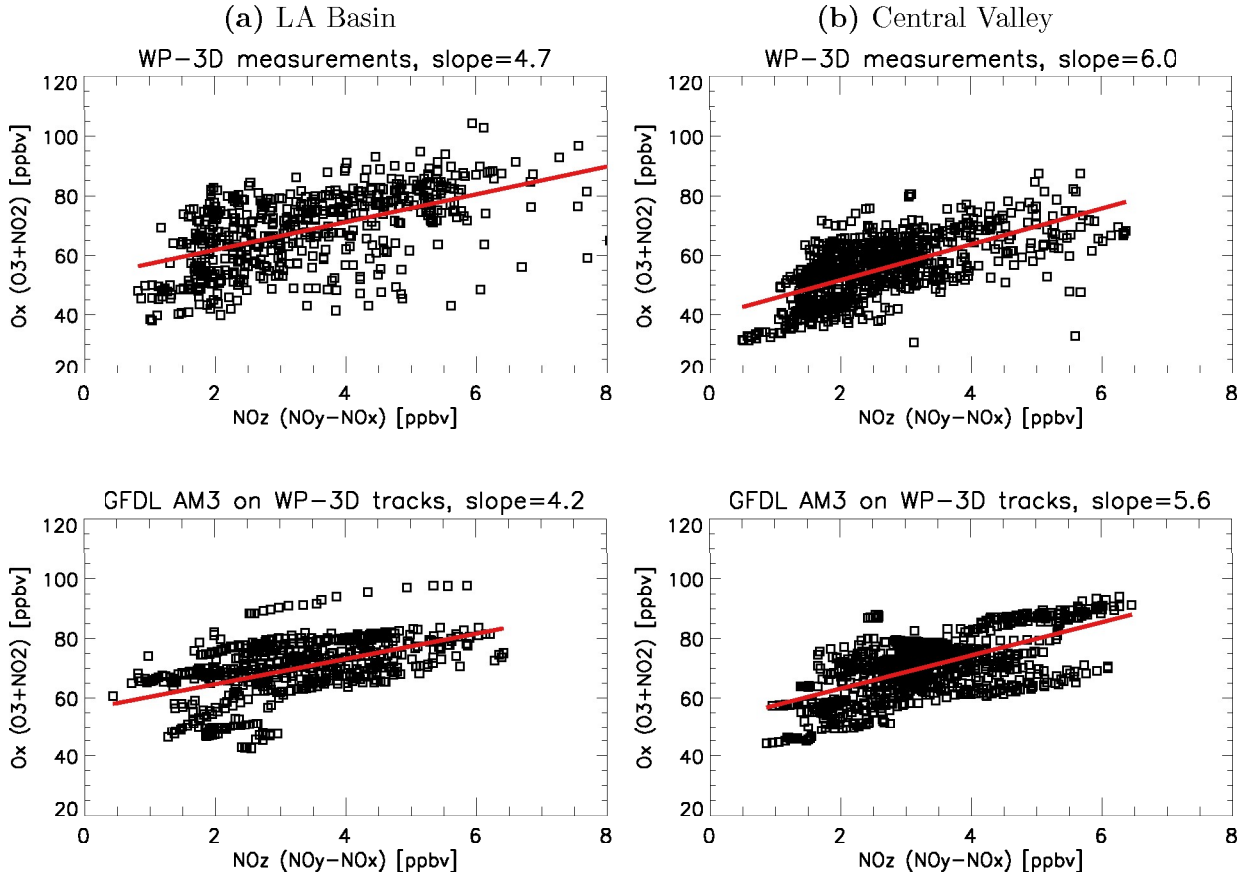

Figure 11. Ozone production efficiency: O_x vs. NO_z from WP-3D daytime measurements and results from the GFDL AM3 model sampled at flight tracks below 1.5 km over (a) the LA Basin and (b) the Central Valley. The slope from the linear regression of O_x to NO_z is given.

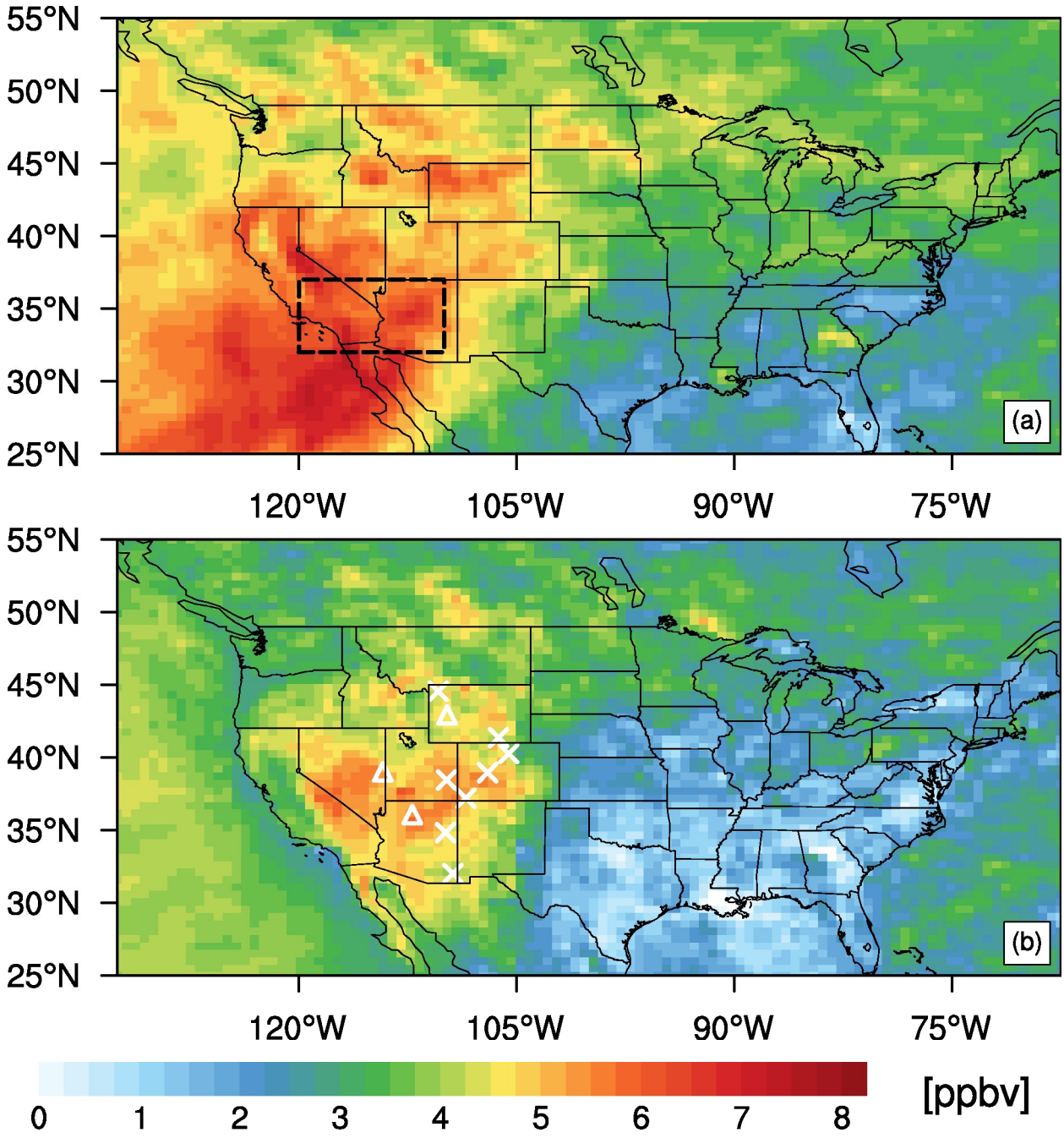

Figure 12. Asian pollution enhancements to (a) mean ozone mixing ratios at ~800 hPa and (b) daily maximum 8-hour ozone in surface air for May-June 2010. The dashed rectangle in (a) indicates the surface region analyzed in Figure 13. The symbols in (b) denote locations of 12 CASTNet high-elevation sites shown in Fig. S5b.

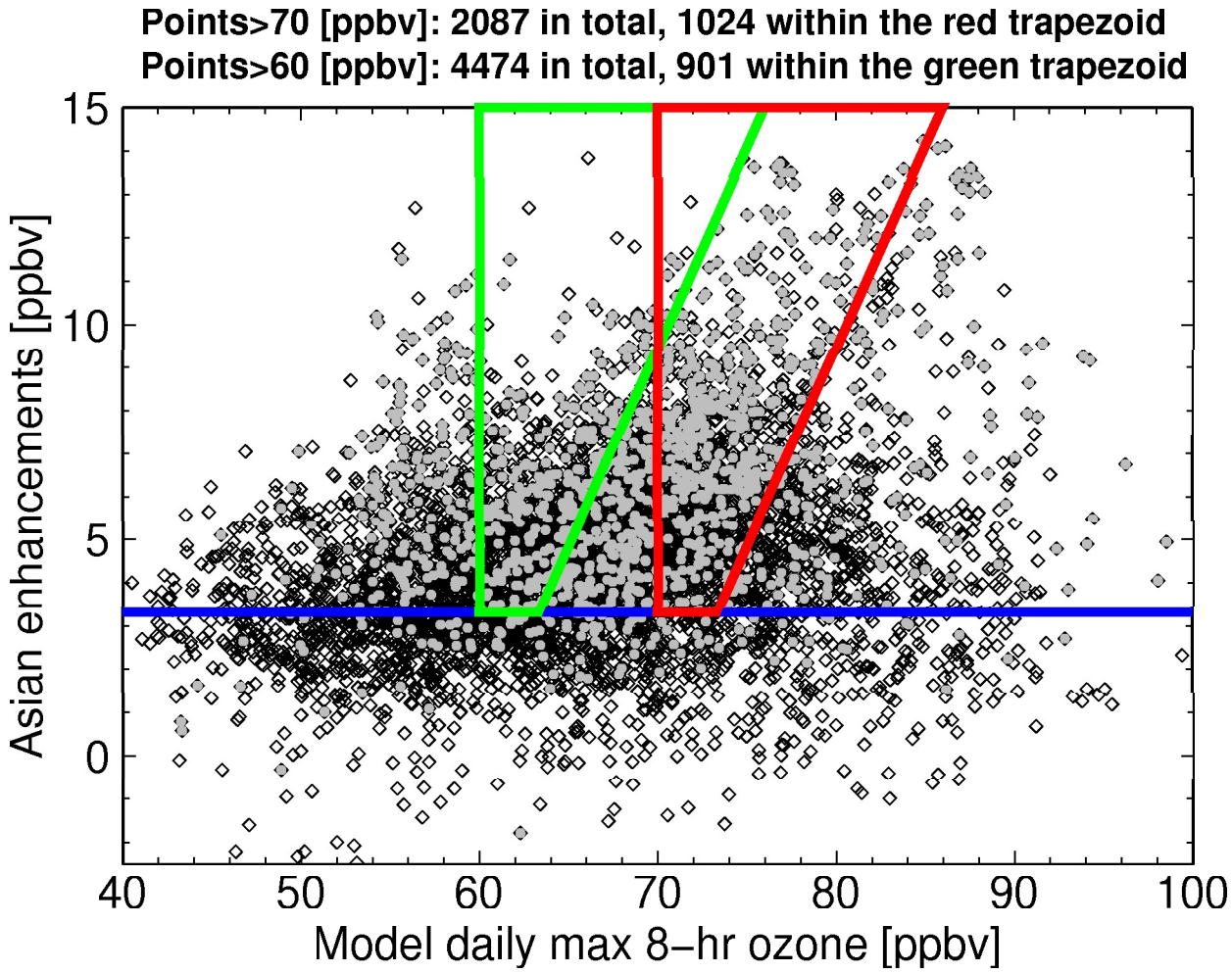

Figure 13. Asian enhancements to daily maximum 8-hour average ozone in surface air, as estimated with the GFDL AM3 model, plotted as a function of total ozone abundances for all land grids within the rectangle indicated in Fig. 12a. The blue line represents the 25^{th} percentile value of Asian enhancements. Points falling within the green and red trapezoids denote values in excess of 60 and 70 ppbv, respectively, that would not have occurred in the absence of Asian emissions in the model. The case study periods in Section 3 are identified as gray points.

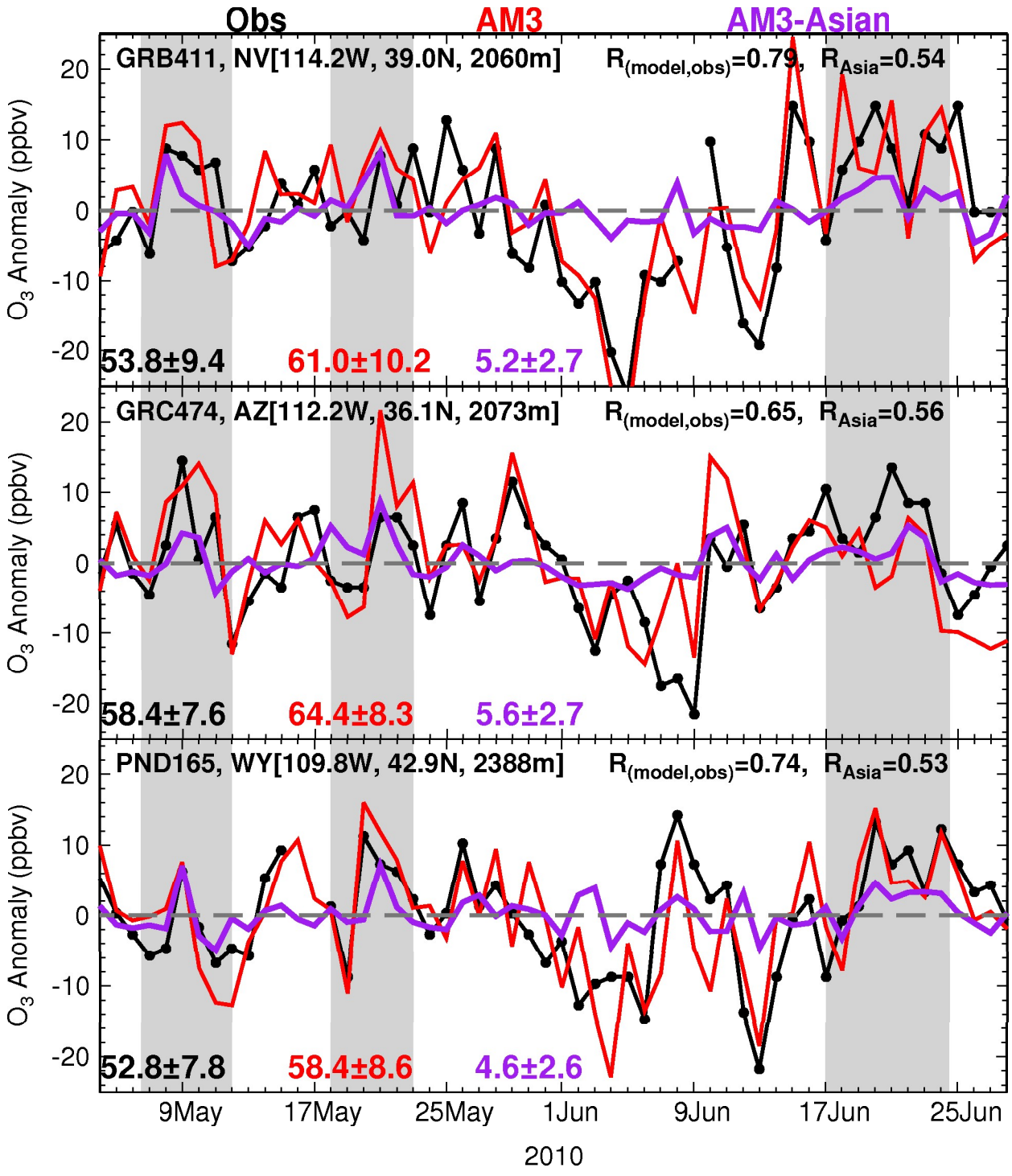

Figure 14. Day-to-day variability of observed (black), modeled (red) and Asian enhancements (purple) to daily maximum 8-hour average ozone at three CASTNet surface stations (triangles in Fig. 12b). Shown are anomalies relative to the May-June mean. The gray shading indicates major Asian pollution events discussed in Section 3.

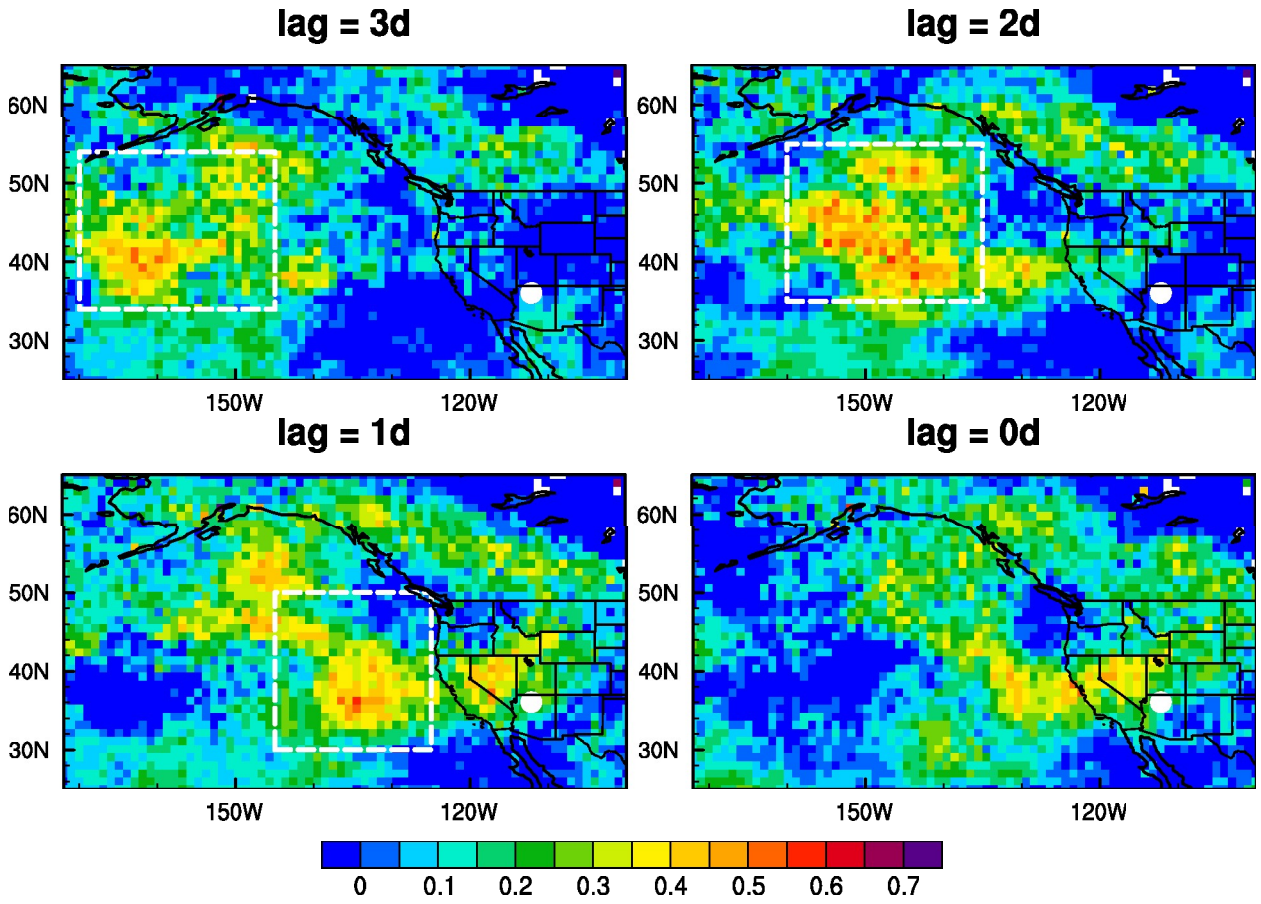

Figure 15. Correlation coefficients between May-June 2010 AIRS daily CO columns at each 1°x1° grid box and AM3 estimated Asian anthropogenic enhancements to daily maximum 8-hour average ozone at Grand Canyon National Park (denoted as a white circle), Arizona, considering time lags of 0-3 days. The rectangles indicate the regions where AIRS CO can be used to derive a space-spaced indicator of Asian influence on surface ozone in the western U.S. (Section 6).

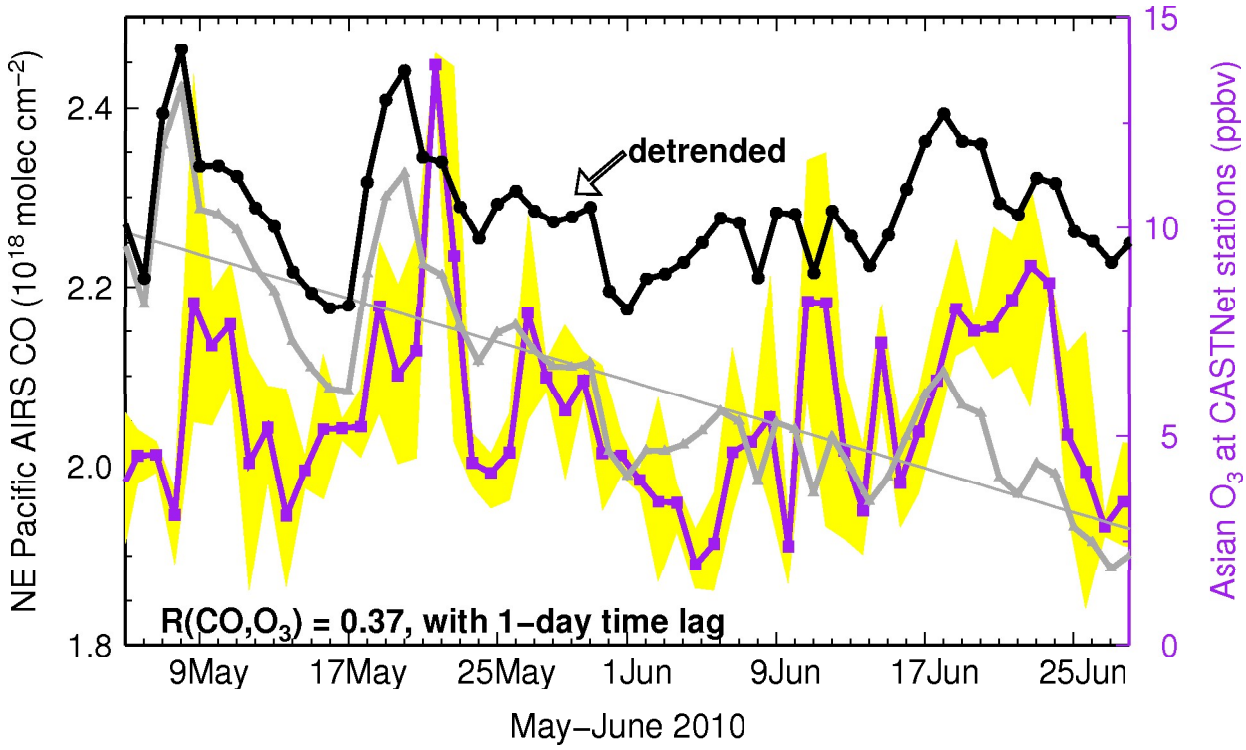

Figure 16. Time series illustrating increasing Asian enhancements to surface ozone (purple) at CASTNet sites following 1-2 days after peak CO columns represented by AIRS (gray, detrended in black) over the eastern North Pacific (30°-50°N, 145°-125°W). The yellow shading indicates the range of Asian enhancements at the three sites, Great Basin, Grand Canyon, and Canyonlands National Parks.

Table 1 May-June 2010 mean statistics for observed and model daily max 8-hr average ozone in surface air at the CASTNet ground stations in the western U.S.

STATE	SITE_ID	SITE_NAME	Elevation (m)	Observed* (ppbv)	Model* (ppbv)	*R*
AZ	GRC474	Grand Canyon NP	2073	59±7	64±8	0.56
AZ	PET427	Petrified Forest	1723	56±7	62±9	0.46
AZ	CHA467	Chiricahua NM	1570	57±7	60±11	0.67
CA	PIN414	Pinnacles NM	335	46±7	62±10	0.83
CA	YOS404	Yosemite NP	1605	53±10	61±10	0.73
CA	LAV410	Lassen Volcanic NP	1756	48±8	60±8	0.80
CA	JOT403	Joshua Tree NP	1244	74±12	72±8	0.42
CA	SEK430	Sequoia NP - Ash Mountain	457	59±13	70±10	0.80
CO	MEV405	Mesa Verde NP	2165	55±8	64±8	0.60
CO	ROM406	Rocky Mtn NP	2743	59±10	61±10	0.72
CO	ROM206	Rocky Mtn NP Collocated	2743	55±11	61±11	0.75
NV	GRB411	Great Basin NP	2060	54±9	61±10	0.71
TX	PAL190	Palo Duro	1050	49±7	54±7	0.46
TX	BBE401	Big Bend NP	1052	49±8	50±7	0.54
UT	CAN407	Canyonlands NP	1809	58±7	65±9	0.57
WA	MOR409	Mount Rainier NP	415	29±8	55±5	0.71
WY	PND165	Pinedale	2388	53±8	58±8	0.69
WY	CNT169	Centennial	3178	56±8	58±8	0.55

* mean ± standard deviation